Department of Applied Physics

Nano- and mesoscale structure control in block copolymers and dendritic supramolecules

Antti Soininen

A!

DOCTORAL DISSERTATIONS

Aalto University publication series
DOCTORAL DISSERTATIONS 24/2013

Nano- and mesoscale structure control in block copolymers and dendritic supramolecules

Antti Soininen

A doctoral dissertation completed for the degree of Doctor of Science (Technology) to be defended, with the permission of the Aalto University School of Science, at a public examination held at the lecture hall E of the school on 24th May 2013 at 12.

Aalto University
School of Science
Department of Applied Physics
Molecular Materials Research Group

Supervising professor
Prof. Janne Ruokolainen

Thesis advisor
Prof. Janne Ruokolainen

Preliminary examiners
Prof. Laurent Rubatat, Université de Pau et des pays de l'Adour, France
Prof. Ritva Serimaa, University of Helsinki, Finland

Opponent
Prof. Ting Xu, University of California, Berkeley, United States of America

Aalto University publication series
DOCTORAL DISSERTATIONS 24/2013

ISBN 978-952-60-5012-6 (printed)
ISBN 978-952-60-5013-3 (pdf)
ISSN-L 1799-4934
ISSN 1799-4934 (printed)
ISSN 1799-4942 (pdf)
http://urn.fi/URN:ISBN:978-952-60-5013-3

Unigrafia Oy
Helsinki 2013

Finland

441 697
Printed matter

Aalto University

Abstract

Aalto University, P.O. Box 11000, FI-00076 Aalto www.aalto.fi

Author
Antti Soininen

Name of the doctoral dissertation
Nano- and mesoscale structure control in block copolymers and dendritic supramolecules

Publisher School of Science

Unit Department of Applied Physics

Series Aalto University publication series DOCTORAL DISSERTATIONS 24/2013

Field of research Applied Physics, Physics

Manuscript submitted 5 November 2012 **Date of the defence** 24 May 2013

Permission to publish granted (date) 18 December 2012 **Language** English

☐ **Monograph** ☒ **Article dissertation (summary + original articles)**

Abstract

The topics of this thesis are self-organized templates, hierarchical structure-within-structure morphologies and induced chirality in solid state assemblies of dendritic molecules. They all contribute to our understanding of the mechanisms of structure formation in the nano- and mesoscale which is key to new materials with unparalleled properties and adaptive functionalities.

In Publications I and II, the microphase separation of diblock copolymers is utilized to template a novolac-type resin to obtain porous carbonaceous material or flakes depending on the initial amount of resin in the mixture. The porous material readily exhibits mesoscale pores which enhance mass transportation while the amount of micropores and thus the total surface area can be controlled by pyrolyzation time. The flakes have high aspect ratio and may have either a solid surface or be covered by polymer brushes ("hairy" flakes) depending on the preparation method.

In Publications III and IV, a second level of structural order is achieved by introducing side-chains to a diblock copolymer. These structures are studied in fixed lamellar morphology on the block copolymer level in bulk and in submicrometer particles. With low side-chain content, side-chains form a single layer sandwiched in the middle of the side-chain block lamellae. This structure changes gradually to liquid crystalline smectic layers ordered perpendicularly to the block domain interfaces as the side-chain content is increased. In the particles, the lamellae form an onion-like morphology except for the high side-chain content block copolymer where the onion-like structure breaks down due to increased splay deformation energy.

Publication V explores the induction of chirality in solid state. Addition of chiral side-chains to three generations of three different types of dendritic molecules leads to nine homologous supramolecules. Structural and optical studies on these cases reveal that the final structures are indeed chiral and that the "strength" of the chirality depends on the quality of the structures. The low generation supramolecules with simpler structures result in better ordered and optically higher-quality morphologies than the higher generation and more complex molecules.

Keywords self-assembly, self-organization, induced chirality, block copolymer, supramolecule, dendron, dendrimer, dendronized polymer

ISBN (printed) 978-952-60-5012-6 **ISBN (pdf)** 978-952-60-5013-3

ISSN-L 1799-4934 **ISSN (printed)** 1799-4934 **ISSN (pdf)** 1799-4942

Location of publisher Espoo **Location of printing** Helsinki **Year** 2013

Pages 139 **urn** http://urn.fi/URN:ISBN:978-952-60-5013-3

A? Aalto-yliopisto

Tiivistelmä

Aalto-yliopisto, PL 11000, 00076 Aalto www.aalto.fi

Tekijä
Antti Soininen

Väitöskirjan nimi
Lohkopolymeerien ja dendristen molekyylien nano- ja mesoskaalan rakenteiden ohjaaminen

Julkaisija Perustieteiden korkeakoulu

Yksikkö Teknillisen fysiikan laitos

Sarja Aalto University publication series DOCTORAL DISSERTATIONS 24/2013

Tutkimusala Teknillinen fysiikka, fysiikka

Käsikirjoituksen pvm 05.11.2012 **Väitöspäivä** 24.05.2013

Julkaisuluvan myöntämispäivä 18.12.2012 **Kieli** Englanti

☐ **Monografia** ☒ **Yhdistelmäväitöskirja (yhteenveto-osa + erillisartikkelit)**

Tiivistelmä

Tämän väitöskirjan aiheina ovat itseorganisoituneet muotit, hierarkkiset sisäkkäiset rakenteet sekä kiraalisten rakenteiden ilmeneminen dendristen supramolekyylien kiinteän olomuodon rakenteissa. Tämä tutkimus auttaa ymmärtämään paremmin nano- ja mesoskaalan rakenteitten syntyä, mikä on erityisen tärkeää suunniteltaessa uusia, ominaisuuksiltaan parempia ja mukautumiskykyisempiä materiaaleja.

Julkaisuissa I ja II käytetään kaksilohkokopolymeerien mikrofaasierottuneita rakenteita novolac-tyyppisen hartsin muottina. Muotilla tuotetaan hiilipohjaista huokoista materiaalia tai lastuja riippuen hartsin ja kopolymeerin sekoitussuhteesta. Huokoinen lopputuote sisältää mikro- ja mesohuokosia. Mesohuokoset parantavat diffuusiota materiaalissa. Mikrohuokoset, joiden määrä voidaan säätää valmistuksessa halutulle tasolle, vuorostaan määräävät materiaalin kokonaispinta-alan. Lastuilla puolestaan on korkea sivusuhde ja niillä on joko sileä tai polymeeriketjujen peittämä pinta (ne ovat "karvaisia") riippuen valmistusmenetelmästä.

Julkaisuissa III ja IV kaksilohkokopolymeerien lamellirakenteisiin sisällytetään toinen, pienemmän mittakaavan rakenne lisäämällä lohkoihin sivuketjuja. Tätä pienempää rakennetta tutkitaan sekä makroskooppisissa ainemäärissä että alle mikrometrin kokoisissa hiukkasissa. Sivuketjut muodostavat yksittäisen kerroksen sivuketjulohkon lamellin sisään, kun sivuketjuja on vähän. Tämä rakenne muuttuu sivuketjuja lisättäessä asteittain smektisiksi tasoiksi, jotka ovat kohtisuorassa kopolymeerin lamelleja vastaan. Pyöreissä hiukkasissa kopolymeeri muodostaa aluksi sipulimaisia rakenteita, joissa lamellit ovat taipuneet pallokuoriksi. Sivuketjuja lisättäessä sipulirakenne kuitenkin hajoaa smektisten tasojen kasvattaessa lamellien taivuttamiseen tarvittavan energian liian suureksi.

Julkaisu V tutkii kiraalisuuden indusoitumista kiinteässä olomuodossa. Liittämällä kiraalisia sivuketjuja kolmen eri generaation kolmeen eri tyyppiseen dendriseen molekyliin saadaan yhdeksän samansyntyistä supramolekyyliä. Optiset mittaukset ja rakenneanalyysi osoittavat, että syntyvät rakenteet todellakin ovat kiraalisia ja että kiraalisuuden "voimakkuus" riippuu siitä kuinka hyvin rakenteet ovat järjestyneet. Yksinkertaisemmat alhaisen generaation supramolekyylit tuottavat paremmin järjestyneitä rakenteita kuin korkeamman generaation monimutkaisemmat molekyylit.

Avainsanat itsejärjestyminen, itseorganisoituminen, indusoitu kiraalisuus, lohkokopolymeeri, supramolekyyli, dendroni, dendrimeeri, dendrinen polymeeri

ISBN (painettu) 978-952-60-5012-6 **ISBN (pdf)** 978-952-60-5013-3

ISSN-L 1799-4934 **ISSN (painettu)** 1799-4934 **ISSN (pdf)** 1799-4942

Julkaisupaikka Espoo **Painopaikka** Helsinki **Vuosi** 2013

Sivumäärä 139 **urn** http://urn.fi/URN:ISBN:978-952-60-5013-3

Preface

I wanted to start this Preface with the words: ”This thesis was written during the hot summer days of 2012” but the summer was rainier than the average and the winter is already coming. Nevertheless, it has been a fun ride. I have also greatly enjoyed my six years as a graduate student in the Group of molecular materials at Aalto University[1] where most of the research for this thesis has taken place. I would like to express my thanks to our professors, Olli Ikkala and Janne Ruokolainen (who was also my supervisor) for providing me all the tutelage as well as the resources necessary for high quality research. Additionally, I want to mention the current and former members of our group I have had the pleasure to work with but the list of individual names would be too long. Yet, you know who you are. It has been great fun to work with you.

Of course, this work would not have been possible without the collaborations with our peer groups. I would like to express my earnest gratitude to professors Nikos Hadjichristidis (National and Kapodistrian University of Athens, Greece), Esko Kauppinen (Aalto University), Helmut Schlaad (Max Planck Institute of Colloids and Interfaces, Germany), Dieter Schlüter (ETH Zurich, Switzerland) and especially to Raffaele Mezzenga (ETH Zurich, Switzerland) and their research groups.

The work for this thesis was partially done in the Center of Excellence of Finnish Academy (”Bio- and Nanopolymers Research Group”, 77317). Additional money has been supplied by the Academy of Finland (projects 128636, 14030, 140362), the European Commission project COMPOSE (NMP3-CT-2003-505633) and the Swiss National Science Foundation.

Last, but definitely not least I would like to thank my friends and relations for this unforgettable experience they call life. You are the best.

[1] Formerly known as the Laboratory of optics and molecular materials in the days of Helsinki University of Technology.

Espoo, Finland, October 17, 2012,

Antti Soininen

Contents

List of Publications

This thesis consists of an overview and of the following publications which are referred to in the text by their Roman numerals.

I A. Soininen, S. Valkama, A. Nykänen, A. Laiho, H. Kosonen, R. Mezzenga and J. Ruokolainen. Functional Carbon Nanoflakes with High Aspect Ratio by Pyrolysis of Cured Templates of Block Copolymer and Phenolic Resin. *Chemistry of Materials*, 19, 3093 – 3095, May 2007.

II A. Soininen, S. Valkama, H. Kosonen, A. Nykänen, R. Ramasubbu, F. Tuomisto, P. Engelhardt, G. ten Brinke, O. Ikkala and J. Ruokolainen. Mono and Bimodal Porosity by Pyrolysis of Block Copolymer-phenolic Resin Complexes. In *Nanoporous Materials Proceedings of the 5th International Symposium*, 347 – 354, March 2008.

III A. Soininen, I. Tanionou, N. ten Brummelhuis, H. Schlaad, N. Hadjichristidis, O. Ikkala, J. Raula, R. Mezzenga and J. Ruokolainen. Hierarchical Structures in Lamellar Hydrogen Bonded LC Side Chain Diblock Copolymers. *Macromolecules*, 45, 7091 – 7097, August 2012.

IV A. Soininen, A. Rahikkala, J. Korhonen, E. Kauppinen, R. Mezzenga, J. Raula and J. Ruokolainen. Hierarchical Structures of Hydrogen Bonded Liquid-Crystalline Side-Chain Diblock Copolymers in Aerosol Particles. *Macromolecules*, 45, 8743 – 8751, October 2012.

V A. Soininen, E. Kasëmi, A. D. Schlüter, O. Ikkala, J. Ruokolainen and R. Mezzenga. Self-assembly and Induced Circular Dichroism in Dendritic

Supramolecules with Cholesteric Pendant Groups. *Journal of American Chemical Society*, 132, 10882 – 10890, July 2010.

Author's Contribution

Publication I: "Functional Carbon Nanoflakes with High Aspect Ratio by Pyrolysis of Cured Templates of Block Copolymer and Phenolic Resin"

The author participated in sample preparation as well as in TEM imaging and SAXS measurements and analysis. A major part of the publication was written by the author and S. Valkama.

Publication II: "Mono and Bimodal Porosity by Pyrolysis of Block Copolymer-phenolic Resin Complexes"

The author participated in sample preparation as well as in TEM imaging except for tomography which was done by P. Engelhardt and A. Nykänen. A major part of the publication was written by the author.

Publication III: "Hierarchical Structures in Lamellar Hydrogen Bonded LC Side Chain Diblock Copolymers"

This work was done in collaboration with the research groups of professors N. Hadjichristidis, R. Mezzenga and H. Schlaad. The author prepared all the supramolecular samples using starting materials part of which were synthesized and analyzed by I. Tanionou. The author carried out TEM, FTIR and SAXS measurements and analysis and wrote a major part of the publication.

Publication IV: "Hierarchical Structures of Hydrogen Bonded Liquid-Crystalline Side-Chain Diblock Copolymers in Aerosol Particles"

This work was done in collaboration with the research groups of professors E. Kauppinen and R. Mezzenga. The author prepared all the supramolecules while the particles were prepared by A. Rahikkala. All subsequent treatments and TEM analysis was done by the author. SEM was done by J. Korhonen. The author also wrote a major part of the publication.

Publication V: "Self-assembly and Induced Circular Dichroism in Dendritic Supramolecules with Cholesteric Pendant Groups"

This work was done in collaboration with the research groups of professors R. Mezzenga and A. Schlüter. The author prepared the supramolecular samples from the dendritic starting materials which were synthesized by E. Kasëmi. All subsequent measurements and analysis were done by the author except for BET which was done by K. Vilonen. A major part of the publication was written by the author.

Nomenclature

γ The angle between the $\vec{a}$ and $\vec{b}$ lattice vectors.

a, b Lattice vector lengths.

$d_{(01)}$ (01) lattice plane distance.

q_1, q_1' Position of the first-order SAXS peak in reciprocal space.

w_{PS} Weight fraction of PS.

x The ratio between side-chains and repeat units of a host polymer block.

BET Brunauer-Emmett-Teller.

CD Circular dichroism.

CholHS Cholesteryl hemisuccinate.

CholSO Cholesteryl sulfate.

DNA Deoxyribonucleic acid.

FTIR Fourier transform infrared spectroscopy.

P4VP Poly(4-vinylpyridine).

PS Poly(styrene).

PS-P4VP Poly(styrene)-*block*-poly(4-vinylpyridine) diblock copolymer.

SAXS Small-angle X-ray scattering.

SEM Scanning electron microscope or microscopy.

TEM Transmission electron microscope or microscopy.

UV-Vis Ultraviolet and visible light spectroscopy.

1. Introduction

New materials with improved properties and novel functionalities are emerging as alternatives to the conventional materials used today. For these materials to be competitive with the conventional ones, they need to provide exceptional performance while being economically viable. Eco-friendliness and sustainability throughout their life cycle from production to disposal is highly desirable as well.

Nature offers several intriguing materials which can be used as inspirational models in the design of new materials. Many materials produced by biological organisms are superior to the ones we conventionally use in terms of their mechanical and physical properties. These materials exhibit multiple properties such as high tensile strength and toughness [1, 2] simultaneously optimized for their function. This is usually hard to achieve by ”simple” materials alone. Thus, multicomponent materials with complex structures are commonly found in nature. Some biological structures alone provide specific functionalities such as the anti-fouling surface patterns of lotus leafs [3] or the color creating structures on butterfly wings [4].

Complex structures involving several length scales are a distinguishing feature of many high performance or functional materials. Because of this, establishing relationships between these structures and the properties they bring is of great importance. This knowledge enables the design of unprecedented materials. Special traits tailored directly into the materials such as self-healing, embedded sensory and adaptation to environment, may some day revolutionize the way we think of the normally inanimate matter around us.

A throughout understanding of the forces and interactions driving the formation of structures on different length scales is therefore the key to the realization of new materials with desired properties and functionali-

ties. This thesis contributes to this end by experimentally exploring how different structures result from the properties and interactions of starting materials and how these structures can be used as templates for other materials. The phase separation phenomenon of block copolymers called microphase separation and liquid crystalline ordering are used here as the forces driving the structure formation. These processes lead to structures on the nano- and mesoscopic length scales. Because the formation of these structures does not require external interference to proceed the resulting structures are often termed as self-organized or self-assembled. The self-organization process can be controlled by external parameters such as temperature or by internal parameters such as lengths of polymer chains. Here, reversible non-covalent bonding is utilized to enable easy control over some of the internal parameters and further to more extensively probe the parameter space available.

This is a compilation thesis which combines the contributions of five different publications. The whole subject is split into three parts which are covered as follows:

Creating flakes and porous materials from block copolymer templates is the topic of Chapter 2 and covers Publications I and II.

Adding complexity to the block copolymer structures by structure-within-structure assemblies in bulk and in spherical submicrometer sized particles is discussed in Chapter 3 and covers Publications III and IV.

The manifestation of chirality of molecular building blocks in higher level structures is the topic of Chapter 4 and covers the last publication, Publication V.

The building blocks used in each topic and the molecular and higher level assemblies they lead to are presented in Figure 1.1. The block copolymer templates and hierarchical structures of Publications I – IV (Chapters 2 and 3) utilize chemically identical diblock copolymers and thus the same microphase separation phenomenon. The end results are different, however, as in the former case the block copolymer is used to shape a curable resin in the mesoscale while the latter case ends up with self-organized hierarchical structures. Very similar cholesteryl side-groups as used for these hierarchical structures are utilized in Publication V (Chapter 4) as well, but this time the side-groups induce chirality to assemblies of dendritic molecules instead of introducing structural complexity.

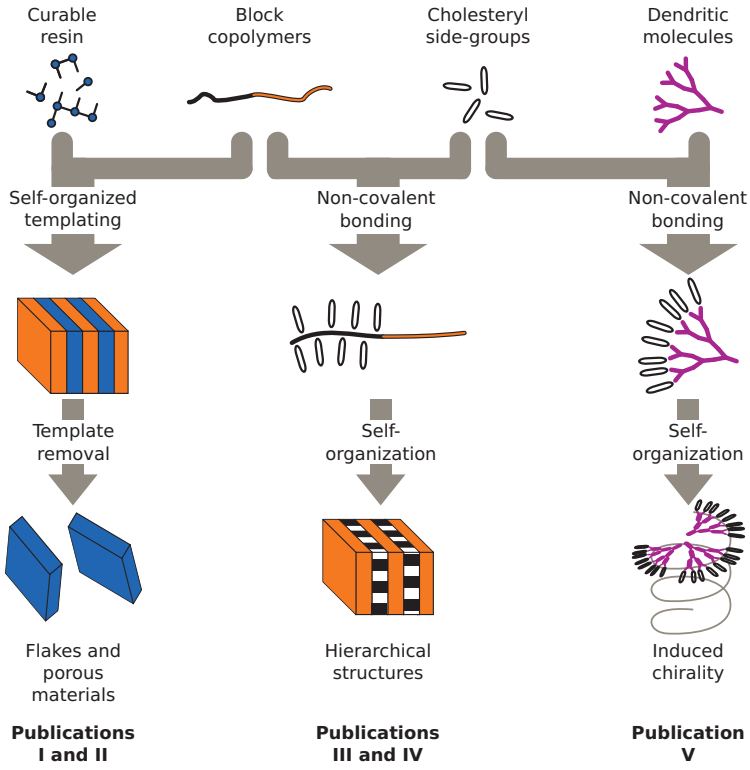

Figure 1.1. The three main topics of this thesis, their starting materials and the processes used to reach the desired structures.

2. Self-organized templates

In this chapter, we will discuss how block copolymers can be used as templates for structures and objects in the mesoscale, that is, in the size range of 10 – 1000 nm. This subject is covered by Publications I and II. Publication I studies the creation of 20 – 30 nm thick and a few micrometers wide flakes from block copolymer templated resin. The same templating process is utilized in Publication II to make hierarchically porous materials.

2.1 Microphase separation of block copolymers

Block copolymers are macromolecules consisting of one or more blocks of different polymers linked together. In this chapter and later in Chapter 3 we restrict the meaning of the term "diblock copolymer" to a block copolymer which consists of two amorphous coil-like blocks A and B which are linked together from their ends.

Macroscopic phase separation of the polymer blocks is impossible because of covalent bonding between the blocks. Instead, the blocks may phase separate in much smaller length scale leading to mesoscopic domains which are rich in one block. This phenomenon is known as *microphase separation*. Typically the characteristic size of the microphase domains is from ten to a few hundred nanometers.

The size and shape of the microphase separated domains depends on the mutual interactions of the blocks and their relative occupied volumes (volume fractions[1]). A phase diagram showing the most common microphase separated structures (or *morphologies*) of diblock copolymers are presented in Figure 2.1. As can be seen from the figure, there will be no

[1]In this thesis, weight fraction w is frequently used because the densities of the constituents are not always known. However, since the densities of organic molecules are usually close to each other, the correspondence between the two is generally quite good.

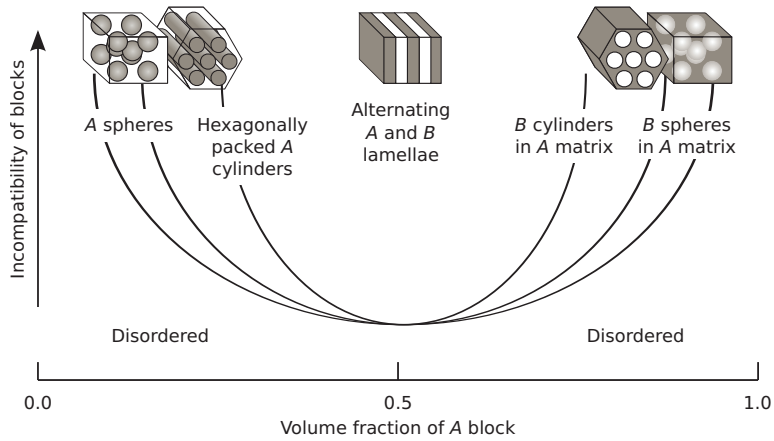

Figure 2.1. Phase diagram showing the most common morphologies found in *AB* type diblock copolymers (*A* gray, *B* white).

microphase separation if there is not enough incompatibility between the blocks or if the *A* block is significantly shorter or longer than the *B* block (volume fraction of *A* is close to zero or unity). Microphases with curved interfaces (spheres or cylinders), on the other hand, are encountered when the lengths of the *A* and *B* blocks are somewhat asymmetrical. Close to symmetric block chain lengths (volume fraction around 0.5) alternating *A* and *B* lamellae are found.

The polymer chains need to be mobile for the microphase separation to take place. Sufficient mobility can be provided by keeping the temperature above the glass transition temperatures of the blocks. Another option is the addition of a solvent which acts as a plasticizer. The solvent can be evaporated which essentially freezes the morphology[2].

2.2 Block copolymers as self-organized templates

Additives can be included selectively to the microphase separated domains which allows exact tailoring of the final morphology. Molecules miscible with the *A* block but not with *B* concentrate in the *A* rich domains increasing the volume fraction of these domains. This may lead to change in the overall morphology if the phase boundaries are crossed.

The additive adapts the shape of the microphase separated domains it is included in. Essentially, the block copolymer acts as a *self-organized template* giving a shape to the additives. For example, Wiesner and his

[2]Often called evaporation induced self-assembly (EISA).

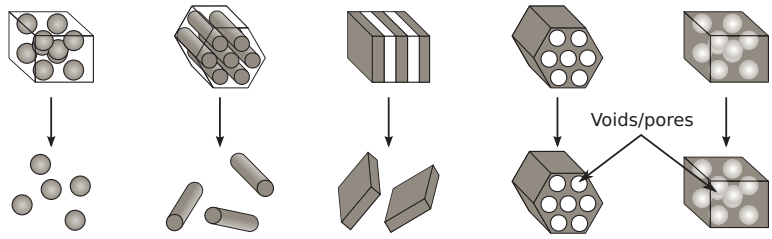

Figure 2.2. Examples of mesoscopic objects and porous materials which can be obtained by block copolymer templating.

group have utilized this phenomenon to template mesoscopically structured inorganic objects and materials. [5, 6, 7] By controlling the amount of precursor mixed with the template block copolymer, they could produce most of the morphologies shown in Figure 2.1 (except for *A* spheres in *B* matrix, in which case a worm-like morphology was observed instead). Subsequent polycondensation of the precursor formed inorganic networks inside the block copolymer domains. Figure 2.2 shows some of the different objects and porous materials which could be obtained this way. If the precursor was confined in spherical, cylindrical or lamellar domains, inorganic spheres, cylinders or flakes could be produced by dispersing the material in a solvent or by pyrolyzation of the block copolymer at high temperatures. In the case of objects dispersed in a solvent, the objects were covered with a layer of the block immiscible with the precursor and were termed ”hairy” objects. Pyrolyzation, on the other hand, removed the block copolymer template completely. If the precursor was confined in the matrix domain, pyrolyzation resulted in a porous inorganic material.

As can be seen from the examples above, block copolymer templates offer versatile and easy way to produce mesoscale objects and pores. The shapes of the objects can be controller directly by the volume fractions of the different constituents while their sizes are determined by the total molecular weight of the block copolymer. The microphase separation of block copolymers is part of so called ”soft” templating methods. [8, 9, 10] The advantage of soft templating over the alternative ”hard” templates [11] which are conventionally used in mesoporous inorganic materials is that presynthesizing a sacrificial template is not required. In the following section, applications of the block copolymer templating method in general and experimental results regarding to this thesis in particular are discussed in detail.

2.3 Templated pores and flakes

Membranes with low gas permeation rates are important in many applications. For example, controlling oxygen diffusion in food packing materials ensures long shelf life. Additionally, special properties such as transparency are desirable for packages intended for consumers. For sustainability, renewable and biodegradable materials should be preferred. One such widely used packaging material is poly(lactide), but it is brittle and has poor gas barrier properties. Fortunately, a plethora of innovative filler particles are being developed which enhance the gas barrier properties and sometimes even robustness of the materials. [12, 13, 14]

The most important mechanism which prevents gas from diffusing through a composite gas barrier membrane is the tortuous path the gas molecules have to take to get around the filler particles according to models and simulations. [15, 16, 17] To maximize this effect, the aspect ratio of the particles has to be high, that is, they need to be plate-like *flakes*. These flakes in turn need to be oriented in plane with the membrane, they need to be imbricated and be impenetrable to the gas molecules.

Some of the more widely studied gas barrier fillers are clay flakes in clay/polymer composites[3]. [18] Being only 1 nm thick but around 100 – 1000 nm wide they pass the first criteria for gas barrier fillers: high aspect ratio. Further, they are inexpensive, non-toxic and relatively easy to exfoliate. In addition to food packaging, clay/polymer composites have shown increased barrier properties in protecting organic solar cells [19], preventing crossover of hydrogen and methane in the proton exchange membranes of fuel cells [20, 21] and in blocking air leaking out of natural rubber tires [22]. Also, carbon and carbon based materials have recently gained attention as prospective alternative to their inorganic counterparts due to their unique properties. [23, 10] Emerging applications for carbonaceous materials include gas separation [24, 25] and capture [26, 27] and energy conversion [28] and storage [29, 30].

If the filler flakes were porous, and the pores would selectively let only certain gas molecules to pass, a membrane would function as a gas separator instead of barrier. Different types of fillers (also granular-shaped) are currently under development. [31, 32] The selective layer in industrial separation membranes is usually only a few hundred nanometers thick because high gas permeation rate is essential for economically viable

[3] Sometimes referred to as mixed matrix membranes (MMM).

products. Therefore, the size and shape of the fillers needs attention and mesoscopically thin flakes, such as porous aluminophosphate [33], seem to be the perfect candidate.

Porous materials have also a plethora of other uses. Many significant phenomena such as adsorption of gas molecules, catalysis and charge separation take place at surfaces. The area of the surface directly influences the efficiency and rate of such phenomena. Therefore, materials with high specific surface areas are needed for practical applications. To date, surface areas of 2000 m^2/g are routinely reached the record being as high as 7000 m^2/g in a metal-organic framework material [34]. The high surface area materials have very high *microporosity* (pore diameter less than 2 nm). However, the small pore size may limit diffusion and the pores are prone to clogging. These problems can be overcome by introducing *meso-* (pore diameter $2-50$ nm) and *macropores* (pore diameter over 50 nm) which promote diffusion. [35] Thus, the key for successful high surface area materials is hierarchic porosity with a mixture of micropores giving large surface area and larger pores for enhanced mass transportation.

Here, the templating method based on block copolymer microphase separation introduced by Kosonen et al. [36] is employed to create carbon based high aspect ratio flakes and porous materials with controllable micro- and mesoporosity. A poly(styrene)-*block*-poly(4-vinylpyridine) diblock copolymer (PS-P4VP) is used as a template and a novolac-type Resin as a cross-linkable carbon source. The Resin is essentially miscible with the P4VP blocks only with which it forms hydrogen bonds.

The amount of Resin added defines the weight fractions of the PS and P4VP(Resin) phases and thus the final morphology. The templating process is schematically shown in Figure 2.3. The starting point of the flakes is the lamellar morphology. The flakes can be ”exfoliated” from the template after curing[4] of the resin by two different ways (Figure 2.3a): They can be separated either by dispersing in a solvent which leaves a layer of PS on the surface of the flakes leading to ”hairy” flakes or by pyrolyzation which turns the Resin into carbonaceous material and removes the PS domains by thermal degradation. For the porous materials, a morphology with cylindrical PS domains is required (Figure 2.3b). Heating the cured template to the pyrolyzation temperature removes the sacrificial PS cylinders leading to mesopores. Intriguingly, prolonged heat treatment at the

[4]Also called hardening or cross-linking.

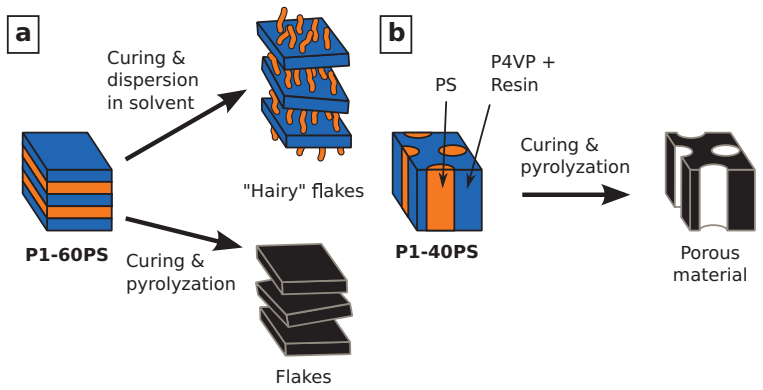

Figure 2.3. a) Block copolymer templated high aspect ratio flakes can be separated by two methods: dispersing in a solvent results in "hairy" flakes while pyrolyzation leads to carbonaceous flakes. b) Mesoporous carbonaceous material can be pyrolyzed from Resin templated by block copolymer with cylindrical morphology.

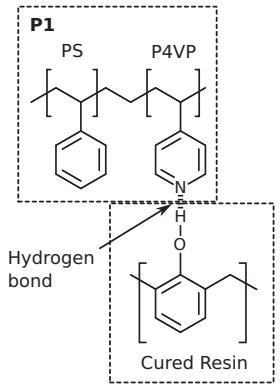

Figure 2.4. Chemical structures PS-P4VP diblock copolymer P1 and Resin molecules.

final pyrolyzation temperature removes the P4VP chains as well resulting in micropores in the pyrolyzed Resin phase. This enables control over the microporosity of the material.

The molecular structures of the templating PS-P4VP diblock copolymer P1 and the novolac-type resin are shown in Figure 2.4. The initial PS weight fraction (w_{PS}) in the pure P1 is 0.88. The TEM image of this copolymer shown in Figure 2.5a shows that its microphase separated structure consists of spherical P4VP domain in PS matrix. This morphology is due to the asymmetric block lengths (see the schematic phase diagram in Figure 2.1).

The addition of Resin which mixes with P4VP decreases the weight fraction of PS. At w_{PS} = 0.60, the lamellar morphology shown in Figure 2.5b

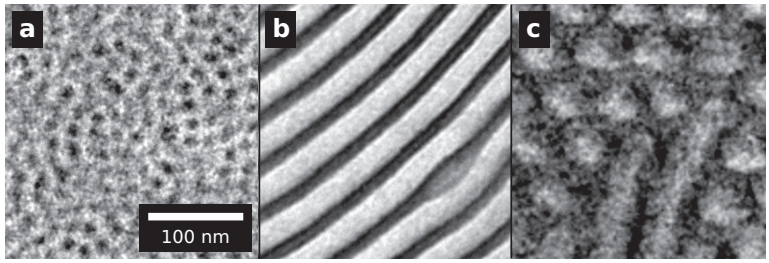

Figure 2.5. TEM images of PS-P4VP diblock copolymer P1 with different Resin contents. a) The pure P1 has spherical P4VP domains in PS matrix. Addition of Resin leads to b) lamellar morphology and c) hexagonally packed PS cylinders in P4VP(Resin) matrix. Iodine staining renders the domains containing P4VP dark. Parts of the figure reprinted with permission from Publication I. Copyright 2007 American Chemical Society.

can be observed. This material will be called P1-60PS hereafter, and it is the starting material for the flakes. Further addition of Resin until the weight fraction of PS decreases to 0.40 results in P1-40PS with hexagonally packed PS cylinders as the TEM image in Figure 2.5c shows. In the ideal case, one would expect a lamellar morphology at this PS weight fraction. However, the cylindrical morphology of P1-40PS is not unusual since the interaction between the blocks and additives also play a major role in the microphase separation and the phase boundaries may become asymmetrical compared to the ideal model phase diagram shown in Figure 2.1.

The Resin phase in the PS-P4VP(Resin) templates is cured step-wise at different temperatures the last (and highest temperature) step being two hours at 190 °C. During the curing, the Resin is cross-linked which also fixes the macroscopic shape of the material. If desired, the pyrolyzation proceeds from here by heating the material at a rate of 1 °C/min until the final pyrolyzation temperature of 420 °C is reached. No protective atmosphere is used.

The lamellar morphology of the template material for the flakes, P1-60PS, is rather well-ordered as the TEM image in Figure 2.6a shows. The morphology is also confirmed by the equally spaced SAXS peaks shown in Figure 2.6b. The position of the first order peak, q_1, at $0.136\,\mathrm{nm}^{-1}$ gives a lamellar period of 46 nm. Even the seventh order peak can be distinguished from the SAXS data which is also a sign of long coherence length in the material.

The well-ordered morphology of the template results in flakes with lat-

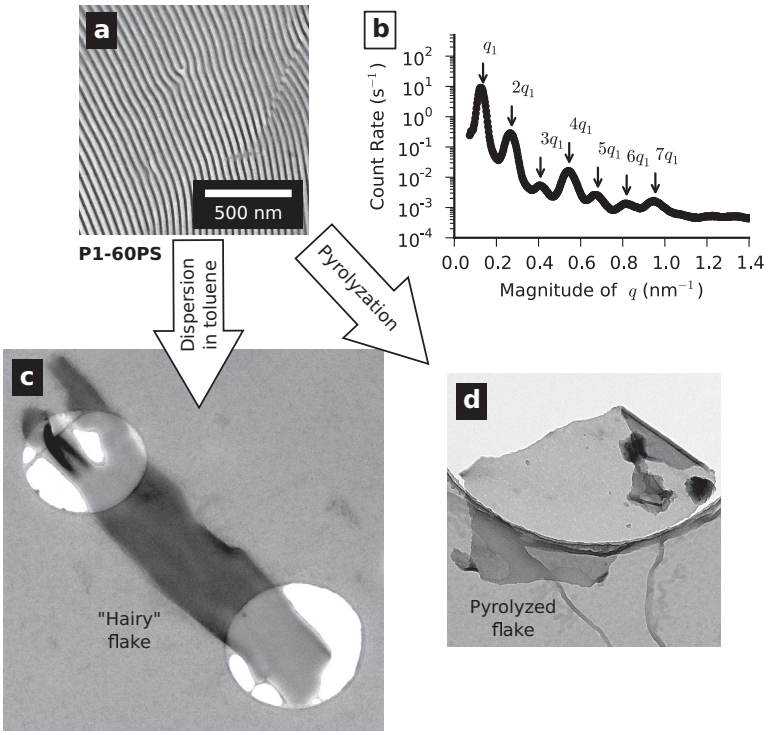

Figure 2.6. a) TEM image of the lamellar morphology of the diblock copolymer templated Resin material P1-60PS. b) SAXS intensity curve of the same material shows several equally spaced scattering peaks. c) TEM image of a ”hairy” flake produced by dispersing cured P1-60PS into a solvent. d) TEM image of a carbonaceous flake produced by pyrolyzation of cured P1-60PS. In the TEM images, iodine staining renders the domains containing P4VP dark. The scale bar is common to all three TEM images. Adopted with permission from Publication I. Copyright 2007 American Chemical Society.

eral dimensions of several micrometers. Figures 2.6c and d show TEM images of flakes produced from the P1-60PS mixture by the two methods: dispersing in solvent and by pyrolyzation. Figure 2.6c shows a single ”hairy” flake which results from dispersing P1-60PS in toluene after curing of the Resin. Toluene detaches the P4VP(Resin) lamellae whose shape is fixed by the curing step leaving them covered with a layer of PS blocks. The PS layer can be seen as the blurry edges of the flake in Figure 2.6c. The thickness of the ”hairy” flakes should be close to the lamellar period of 46 nm. Pyrolyzation of P1-60PS, on the other hand, results in flakes such as the one shown in Figure 2.6d. This flake consists only of cured and pyrolyzed P4VP(Resin). The lack of PS around the flake is evident from the sharp edges of the flake compared to the ”hairy” flake in Figure 2.6c.

In the case of the P1-40PS mixture with the cylindrical morphology, py-

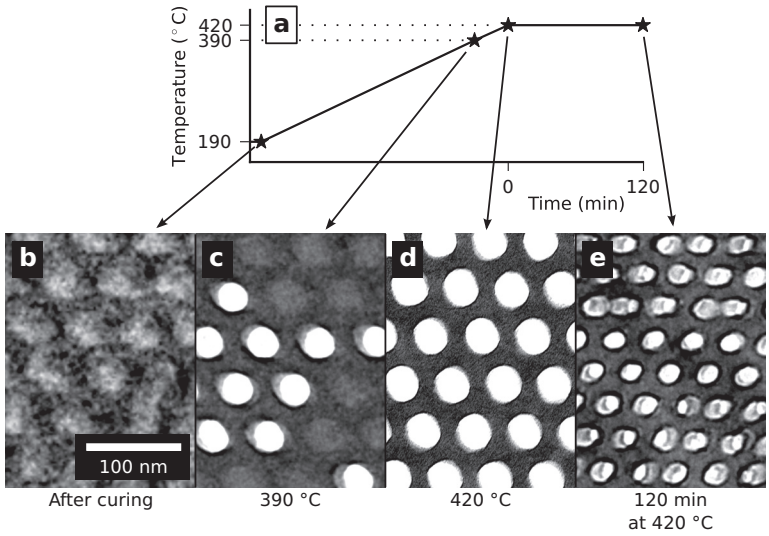

Figure 2.7. TEM images of the progress of pyrolyzation of the diblock copolymer templated Resin material P1-40PS. a) Temperature profile of the pyrolyzation process after the last curing step at 190 °C. b) In the cured template, PS forms hexagonally packed cylinders in P4VP(Resin) matrix. c) Heating the material to 390 °C leads to partial removal of PS. d) At 420 °C, most of the PS is removed. e) After 120 minutes at 420 °C, the material shows signs of collapsing as the dimensions of the mesoscale structure shrink visibly. In the TEM images, iodine staining renders the domains containing P4VP dark. Parts of the figure reprinted with permission from Publication II. Copyright 2008 World Scientific.

rolysis at 420 °C after the curing of the Resin removes the cylindrical PS domains leaving pores of 20 – 30 nm in diameter according to TEM. The progress of the pyrolyzation is illustrated in the series of TEM images in Figure 2.7. The images in the series are taken from samples whose pyrolyzation process was discontinued at different points of the temperature profile shown in Figure 2.7a. The first TEM image in Figure 2.7b shows the yet intact cylindrical PS domains in a cured P4VP(Resin) matrix. At 390 °C, part of the PS domains are already removed (Figure 2.7c) and, at 420 °C, almost all PS is gone (Figure 2.7d). Keeping the material at 420 °C for 120 minutes leads to partial collapse of the structure (Figure 2.7e). According to Valkama et al. [37], the structure stays intact until 60 minutes at 420 °C. Thus, the collapse takes place between 60 and 120 minutes at this temperature.

The porosity of P1-40PS can be analyzed using gas adsorption techniques. Nitrogen adsorption isotherms of the material after heating to 390 °C and to 420 °C, and after 30 and 120 minutes at 420 °C are shown in Figure 2.8a. The sharp increase in adsorbed volume near the relative

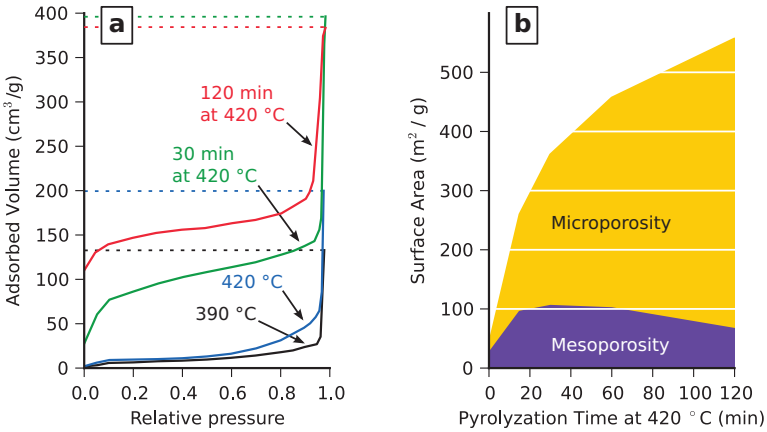

Figure 2.8. a) Nitrogen adsorption isotherms of the P1-40PS mixture after different pyrolysis conditions. b) Micro- and mesopore surface areas of P1-40PS after different pyrolyzation times at 420 °C.

pressure of 1.0 in all isotherms is indicative for multilayer nitrogen adsorption at the pore walls and hints to meso- and macroporosity. This porosity is due to the mesopores left by the removal of PS. The final adsorbed volume is relatively low in the 390 °C and 420 °C samples compared to the samples which received longer heat treatment at 420 °C. This is because PS is not completely removed from the less pyrolyzed templates which results in partially filled and inaccessible pores. The samples pyrolyzed for 30 and 120 minutes at 420 °C show also an adsorption plateau in the intermediate relative pressure range 0.2 – 0.8 which is a sign of microporosity. This plateau is missing in the less heat-treated samples.

The surface areas of micro- and mesopores can be deduced from the nitrogen adsorption isotherms by the BET method. The evolution of the surface areas during the pyrolysis at 420 °C are compiled in Figure 2.8b. As can be seen, a total surface area of over 500 m^2/g can be achieved. The surface area of mesopores reaches maximum after 30 minutes of pyrolyzation at 420 °C. At this point all the PS is removed from the sample. After that, the mesopore area starts to decline. This is most certainly due to the collapse of the material (see Figure 2.7e). The micropore area, on the other hand, increases until the maximum pyrolyzation time of 120 minutes. According to Valkama et al., the micropores are due to removal of the P4VP chains from the P4VP(Resin) matrix. [37] Thus, the P4VP(Resin) matrix is also degraded during the pyrolyzation ultimately leading to the collapse of the material.

2.4 Summary

The morphology of the PS-P4VP diblock copolymer P1 can be changed from spherical to lamellar and further to cylindrical by adding Resin which is selectively incorporated into the P4VP phase. After curing the Resin, flakes from P1-60PS can be exfoliated by dispersing the cured material in a solvent or by removing the sacrificial PS lamellae by pyrolyzation. The resulting high aspect ratio flakes could be used, for example, in gas barrier membranes. The final porosity of pyrolyzed P1-40PS, over 500 m^2/g, is in the league of similar materials. The microporosity can be safely tuned from 0 m^2/g to approximately 400 m^2/g before the mesoporous structure starts to collapse. If the collapse and shrinkage of the material are not issues, even higher specific surface areas may be achievable.

3. Hierarchical self-organization

Self-organized structures are not limited to a single length scale. Nested structures with multiple length scales are ubiquitous for example in biological systems. In this chapter an additional level of structural complexity is added to the microphase separated morphologies of block copolymers presented in the previous chapter. The subject is covered in part by Publication III which studies these hierarchical structures in bulk and in part by Publication IV which explores them in spherical particles.

3.1 Supramolecular side-chain polymers

Non-covalent bonds, such as the hydrogen bond, enable reversible binding of molecular building blocks into larger entities called *supramolecules* without tedious chemical reactions. Probably the most famous supramolecules are DNA molecules which consist of two macromolecular strands bonded together by non-covalent hydrogen bonds.

The reversibility of the non-covalent bonds is one aspect which makes them so intriguing in the application point of view. As their binding energies are of the order of the thermal energy at room temperature, the bonds can be relatively easily broken by mild external stimuli such as a change in temperature. This allows design of ”smart” materials with prominent or even unconventional responses to changes in their environment which further enables dynamic control over the properties of the material. [38]

There are basically two types of supramolecular polymers: either the repeat units themselves are non-covalently linked [39, 40] or molecules are non-covalently attached to a host polymer backbone as side-chains [41, 42, 43]. Here, we will focus on the non-covalent side-chain type also shown in Figure 3.1a.

In bulk, side-chain polymers usually stack in alternating layers of back-

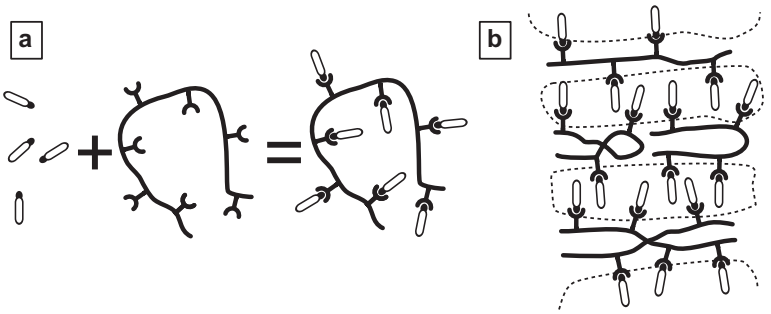

Figure 3.1. a) Non-covalent attachment of side-chains to a polymer backbone. b) Smectic stacking of resulting side-chain polymers.

bones and side-chains as Figure 3.1b schematically shows. This liquid crystalline smectic ordering is a result of packing of the side-chains and partial stretching of the backbones and it may occur even if none of the components were liquid crystalline. [44, 45] With non-covalent attachment, one can control the density of side-chains along the backbone. This enables for example the control over the smectic layer spacing. [45, 46]

3.2 Confined microphase separation

Generally in block copolymers, the block with the lowest surface energy concentrates at the surface of the material. [47, 48, 49] This surface effect will direct the self-organization process orienting the microphase separated domains along the surface. However, the orientation is usually lost far from surface since the correlation length is relatively short in block copolymers due to defects caused by polydispersity and incomplete equilibration caused by slow chain dynamics.

The surface effects take over the self-organization process when the characteristic size of a piece of a material is smaller than the coherence length of the self-organized structure. In this regard, thin films can be thought as one-dimensional confinement. [50] In thin films, the microphase separated structures may be perfectly oriented in the direction normal to the film surfaces while in the lateral direction where the film extends to macroscopic length scales the structure is ”polycrystalline”. For example, the lamellae of block copolymers with the lamellar morphology orient parallel to the film surfaces. Two-dimensional confinement can be realized, for example, in cylindrical spaces. [50] Inside a cylinder, the lamellar morphology bends to concentric circular shells along the cylin-

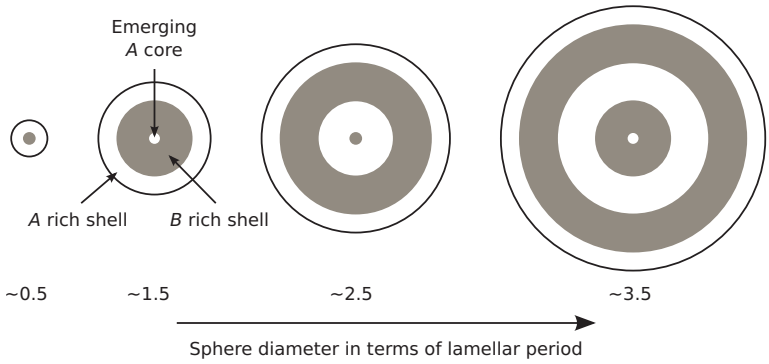

Figure 3.2. The development of the onion-like morphology of symmetric *AB* diblock copolymer inside spherical confinement as a function of sphere diameter.

der axis. The most interesting case considering this thesis is, however, the three dimensional confinement within spherical space.

In the spherical confinement, the lamellar morphology bends along the surface of the confinement creating a series of concentric spherical shells, resulting in an *onion-like structure*. [50] Figure 3.2 shows schematically the theoretical development of the onion-like morphology as the diameter of the spherical confinement increases according to simple volumetric arguments. In the case of diblock copolymers, the thickness of the outermost shell is only about half of that of the inner shells since there is only half of the amount of polymer blocks compared to the inner shells. The thickness of the inner shells, on the other hand, should be close to the lamellar thickness in bulk. Every time the diameter of a spherical confinement grows approximately by the lamellar thickness, a new domain of different polymer block emerges at the center of the confinement as Figure 3.2 shows.

3.3 Hierarchical self-organization in bulk and in spherical confinement

Substructures can be embedded into the microphase separated domains of block copolymers by adding side-chains to the copolymer blocks as explained in Section 3.1. In these systems, the whole block polymer microphase separates in the 10 – 100 nm scale while the side-chain blocks make liquid crystalline structures in the 1 – 10 nm scale. [51, 52, 53] However, as discussed in Section 3.1, when side-chains are added to a polymer they do not have to be liquid crystalline to achieve smectic structures.

There are several examples of self-organization where non-covalently attached side-chains form smectic layers perpendicular to the block domain interfaces. [54, 55, 56, 57, 58, 59, 60, 46]

The reversibility of the non-covalent bonds can be utilized in the side-chain block copolymers as well. [61, 62, 63, 64] It is possible, for example, to use the side-chains as fillers which can be washed away from the block copolymer structure leaving empty pores. [65] Porous thin films made this way could be used as photolitographic masks, for instance. [66, 67] This technique will be used here later to produce mesoporous submicrometer particles. Additional applications of non-covalently attached side-chains could include, for example, photonic band gap materials with reversibly switchable gap. Thermal triggering of such materials has been already demonstrated. [68, 69]

Although there has been a lot of research in the hierarchical structures of side-chain block copolymers, no studies have been published on the development of the liquid crystalline substructure as a function of side-chain content in a constant morphology on the block copolymer level. This is because usually the block copolymer morphology changes as the volume fractions of the blocks are changed (see Section 2.1). Here, the relative lengths of the copolymer blocks in the backbone are chosen such that the morphology stays lamellar throughout the different amounts of side-chains used.

Also, this far side-chain block copolymers and hierarchical self-organization within spherical confinement have not received much attention. [70] Specifically, the liquid crystallinity of the side-chain substructures has not been addressed at all. To remedy the situation, in addition to hierarchical structures in bulk, the self-organization phenomenon inside the spherical confinement is studied here as well.

The PS-P4VP diblock copolymer used in this part of the thesis is chemically the same as the one used to template the Resin in Chapter 2. However, the molecular weights of the PS and P4VP blocks are different and thus the copolymer is called P2. Further, cholesteryl hemisuccinate (CholHS) is used as hydrogen bonding side-chains. Chemical structures of both P2 and CholHS molecules as well as their bonding are presented in Figure 3.3.

The amount of CholHS in the studied supramolecules is represented by x, the ratio between CholHS molecules and P4VP repeat units. Three different ratios are used here. The main properties of the structures of

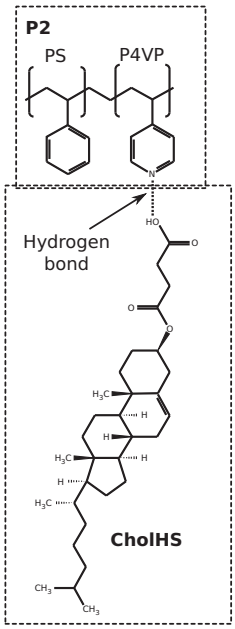

Figure 3.3. Chemical structures of the PS-P4VP diblock copolymer P2 and CholHS side-chains and their mutual hydrogen bonding.

the copolymers in bulk are compiled into Table 3.1.

SAXS and TEM were used to pin down the microphase separated structures and lattice parameters of the materials. SAXS intensity curves and corresponding TEM images of the pure PS-P4VP diblock copolymer P2 and its supramolecular counterparts P2-25CholHS, P2-50CholHS and P2-75CholHS are shown in Figure 3.4. The position of the first order SAXS peak for P2 (Figure 3.4a) gives a (01) lattice plane distance ($d_{(01)}$) of 37.4 nm. The weight fraction of PS, w_{PS}, in P2 is 0.71 which suggests cylindrical morphology. Indeed, in TEM (Figure 3.4b), P4VP cylinders in

Table 3.1. Structural properties of the pure PS-P4VP diblock copolymer P2 and the side-chain PS-P4VP(CholHS) samples. Adopted with permission from Publication III. Copyright 2012 American Chemical Society.

Copolymer	x	w_{PS}	Morphology (TEM)	$d_{(01)}$ (SAXS) (nm)
P2	0.00	0.71	Hexagonal P4VP cylinders	37.4
P2-25CholHS	0.25	0.53	Lamellar	29.5
P2-50CholHS	0.50	0.42	Lamellar	29.5 and 36.0
P2-75CholHS	0.75	0.35	Lamellar	36.0

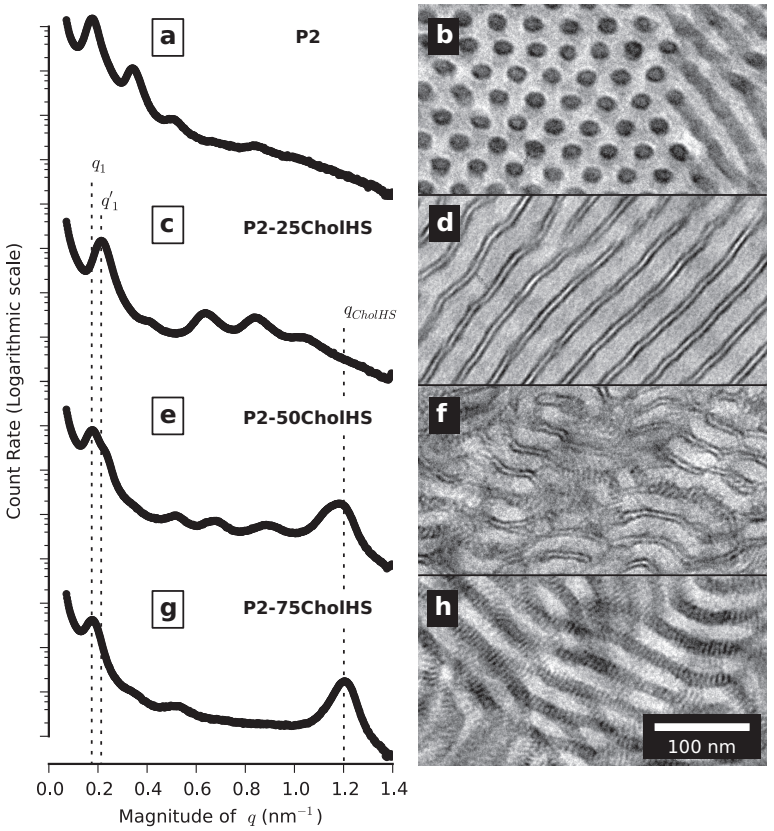

Figure 3.4. SAXS intensity curves and TEM images of a) and b) the pure PS-P4VP diblock copolymer P2, c) and d) P2-25CholHS, e) and f) P2-50CholHS and g) and h) P2-75CholHS. Iodine staining renders the P4VP domains dark. Parts of the figure reprinted with permission from Publication III. Copyright 2012 American Chemical Society.

PS matrix are observed. The cylinders seem to be in hexagonal lattice even though some characteristic SAXS peaks for hexagonal packing are missing, for example at $\sqrt{3}$ or $\sqrt{7}$ times the position of the first-order peak. The absence of these peaks is probably due to minima in the form factor of this particular structure at these scattering vector magnitudes.

All of the supramolecular PS-P4VP(CholHS) samples are lamellar according to both SAXS and TEM, as expected. The (01) lattice plane distance ($d_{(01)}$) of P2-25CholHS given by the first order SAXS peak at q_1', corresponds to the total lamellar period of 29.5 nm (Figure 3.4c). A closer look at the TEM image of P2-25CholHS in Figure 3.4d, reveals an exceptional organization of the P4VP(CholHS) blocks. In P2-25CholHS, the CholHS molecules are packed in a single layer sandwiched between P4VP-rich domains. This layer manifests itself as the thin white stripe inside the

dark P4VP lamellae in TEM. This structure does not originate from liquid crystalline packing of P4VP(CholHS) blocks. Rather, it resembles the triple lamellar microphase separated morphology found in some triblock copolymers. [71, 72, 73, 74]

The single layered CholHS structure found in P2-25-CholHS appears only when the amount of CholHS side-chains attached to the polymer backbone is sufficiently low. Additional side-chains will gradually shift the structure towards the ”conventional” smectic packing. In P2-50CholHS this change is already evident. The SAXS intensity curve of P2-50CholHS shown in Figure 3.4e comprises of peaks from both P2-25CholHS and P2-75CholHS. P2-75CholHS has exclusively the smectic P4VP(CholHS) structure as will be discussed later. Also, the TEM image of P2-50CholHS in Figure 3.4f shows a mixture of features from both P2-25CholHS and P2-75CholHS. The SAXS peak between $1.1-1.2\,\mathrm{nm}^{-1}$ originates from the smectic P4VP(CholHS) layers and its position gives a spacing of 5.3 nm for the layers.

The shift to the smectic P4VP(CholHS) packing is complete in P2-75CholHS. The position of the first-order SAXS peak at q_1 gives a period of 36.0 nm on the block copolymer level (Figure 3.4g). The TEM image in Figure 3.4h confirms the lamellar morphology. In the TEM image, smectic layers of P4VP(CholHS) perpendicular to the block domain interfaces appear exclusively. The pronounced SAXS peak at $q_{CholHS} = 1.20\,\mathrm{nm}^{-1}$ in Figure 3.4g, corresponding to smectic layer period of 5.2 nm, originates from this structure. The magnitude of the smectic period indicates a double-layered packing of the CholHS molecules. [46] The period is also slightly smaller than in P2-50CholHS. This is expected, since the additional side-chains stretch the P4VP blocks which decreases the thickness of the P4VP layers in the smectic packing. [46]

To study how these hierarchical structures manifest in spherical confinement, particles of each block copolymer were produced using an aerosol method. In the aerosol method, a solution of a block copolymer is dispersed in air as small droplets. The solvent evaporates from the droplets quickly leaving solid spherical particles. While some particles with diameters up to a few micrometers are produced, the majority of the particles are in the $100-200$ nm range. The particles are then floated through a heated reactor which enables thermal annealing of the particles. The annealing step removes the effects of the solvent evaporation on the morphology. After the reactor, the particles are cooled down quickly

which may trap the block copolymer morphology to the state it was in the reactor. This allows some morphologies only present at elevated temperatures to be studied and utilized at room temperature.

The same hierarchical structures found in bulk of the block copolymers P2, P2-25CholHS, P2-50CholHS and P2-75CholHS, occur also in the particles prepared using the aerosol method and an annealing temperature of 160 °C in the reactor. Figure 3.5 shows TEM images of typical examples. In the particles, the hexagonal P4VP cylinders of the pure P2 block copolymer turn out as the worm-like structures seen in Figure 3.5a. Also in these particles, PS concentrates on the surface because it has lower surface energy than P4VP.

In the supramolecular side-chain block copolymer P2-25CholHS, the spherical shape of the particles bends the single-layered CholHS structure to the so-called onion-like structure (Figure 3.5b). The CholHS molecules also function as surfactants concentrating the P4VP(CholHS) on the surface of the particles.

With P2-50CholHS as the starting material, particles with both the single-layered CholHS and the perpendicular smectic substructure in the P4VP(CholHS) domains are produced. The overall structure of the particles is onion-like, as well, as Figure 3.5c shows.

Strikingly, the onion-like structure of the particles breaks down in the case of P2-75CholHS. As Figure 3.5d shows, the P4VP(CholHS) domains extend inwards from the surface of the particle. The increased amount of CholHS side-chains in P2-75CholHS compared to P2-50CholHS increases the splay deformation energy of the P4VP(CholHS) domains rendering the bending of the P4VP(CholHS) lamellae into the onion-like morphology energetically too expensive. This forces the self-organization process to find less bent and thus energetically more favorable configurations which results in the breakdown of the onion-like structure.

If the disappearance of the onion-like structure is driven by the liquid crystalline organization of P4VP(CholHS), then the onion-like structure should be reestablished if the liquid crystalline organization was suppressed above the isotropization temperature of the P4VP(CholHS) domains. The isotropization temperature of a similar PS-P4VP(CholHS) diblock copolymer with the lamellar microphase morphology was 162 °C for CholHS to P4VP repeat unit ratio x = 0.75 and 172 °C for x = 1.00 in a previous study by Korhonen et al. [46] Thus, a reactor temperature of 200 °C was deemed to be sufficient to test this hypothesis. The results

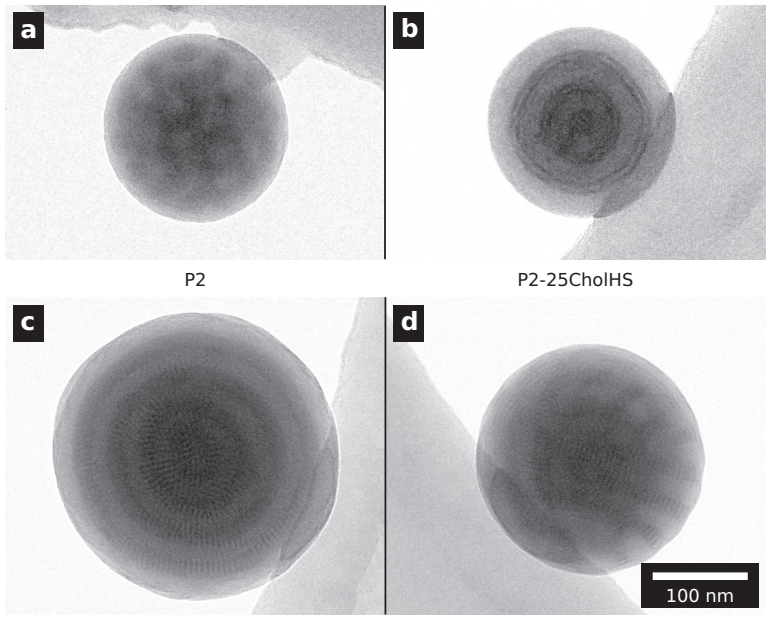

Figure 3.5. TEM images of a) the PS-P4VP diblock copolymer P2, b) P2-25CholHS, c) P2-50CholHS and d) P2-75CholHS particles at the edge of a carbon support film. Logarithm of intensity has been used to enhance the contrast while iodine staining renders the P4VP domains dark. Parts of the figure reprinted with permission from Publication IV. Copyright 2012 American Chemical Society.

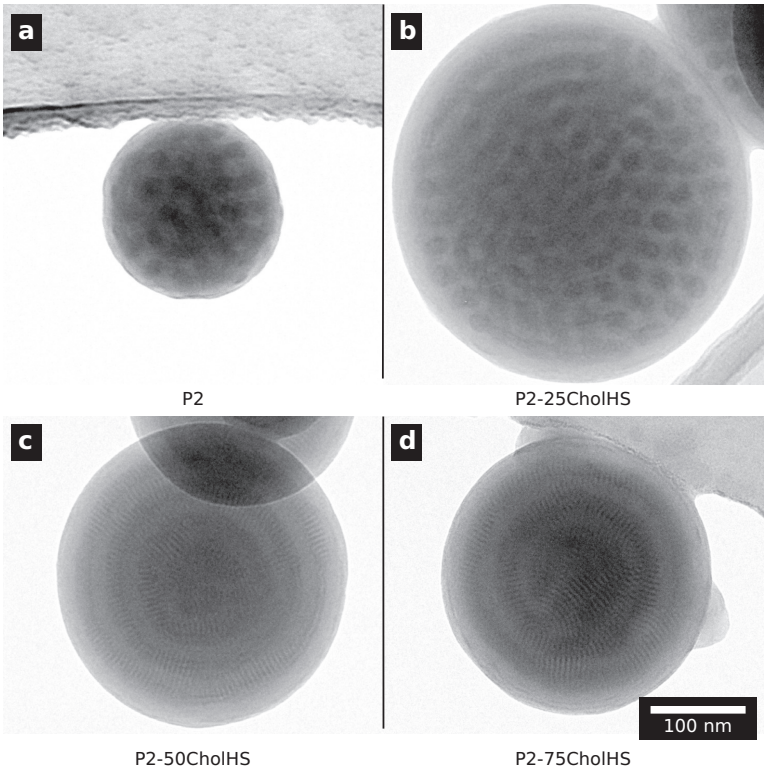

Figure 3.6. TEM images of a) the PS-P4VP diblock copolymer P2, b) P-25CholHS, c) P-50CholHS and d) P2-75CholHS particles produced in aerosol reactor at 200 °C. Logarithm of intensity has been used to enhance the images while iodine staining renders the P4VP domains dark. Parts of the figure reprinted with permission from Publication IV. Copyright 2012 American Chemical Society.

are shown in Figure 3.6. There is no marked difference between the pure P2 particles produced at 160 °C (Figure 3.5a) and at 200 °C (Figure 3.6a), as expected. The same should be true for the P2-25CholHS particles, but the morphology changes unexpectedly when the particles are produced at 200 °C.

Comparison of the P2-25CholHS particles in Figure 3.5b (160 °C) and 3.6b (200 °C) shows that the overall morphology changes from onion-like to cylindrical when the particles are produced at 200 °C. This behavior is probably due to CholHS molecules becoming more soluble into the PS domains or partly evaporating into the aerosol reactor. Indications of CholHS dissolving into the PS domains are also reported by Korhonen et al., who suspected that CholHS molecules migrated into the PS domains of PS-P4VP(CholHS) diblock copolymers during repeated heating and cooling cycles. [46] In the PS-P4VP(CholHS) particles, due to CholHS

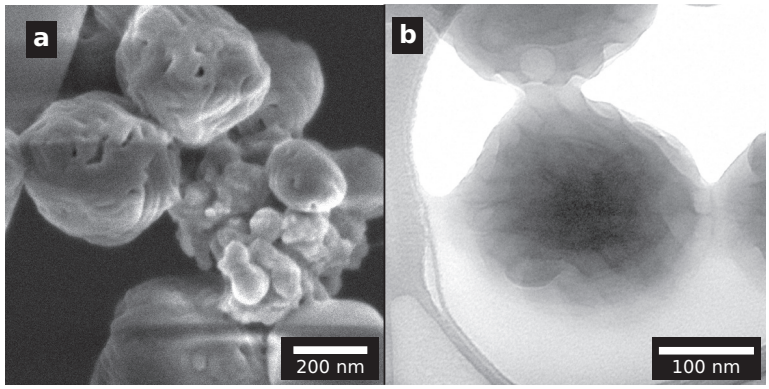

Figure 3.7. a) SEM and b) TEM images of the PS-P4VP(CholHS) side-chain diblock copolymer P2-75CholHS particles after selective removal of CholHS side-chains by ethanol. Adopted with permission from Publication IV. Copyright 2012 American Chemical Society.

migrating into the PS domains or evaporating into the aerosol reactor, the volume fraction of P4VP(CholHS) decreases leading to the observed change in the morphology. Similarly to the single CholHS layer sandwiched between the P4VP rich domains in bulk, a core consisting of CholHS molecules can be observed inside the P4VP(CholHS) cylinders under TEM.

The morphology of the P2-50CholHS particles, on the other hand, does not change significantly when the aerosol reactor temperature is increased to 200 °C. As expect, both the single CholHS layer and smectic P4VP(CholHS) domains are found in the particles as shown in Figure 3.6c.

Lastly, in the P2-75CholHS particles, the morphology indeed changes back to onion-like when the particles are produced at 200 °C. However, it remains undecided whether this change is due to the isotropization of the P4VP(CholHS) blocks or the partial evaporation or mixing of CholHS into the PS domains. The decreasing amount of CholHS in the P4VP(CholHS) domains can explain the onion-like morphology alone as the bending of the domains becomes energetically less expensive allowing the onion-like morphology to reappear.

Subsequent selective removal of CholHS side-chains from the particles proved to be possible. Figure 3.7 shows SEM and TEM images of P2-75CholHS particles produced at 160 °C after ethanol treatment. Unfortunately, the remaining PS ”skeleton” is too soft to support the voids inside the particles which leads to crumpling. The ethanol treatment of P-25CholHS and P-50CholHS particles with the onion-like structure leads

to concentric P4VP-covered PS shells with voids.

3.4 Summary

The hierarchical structures found in the PS-P4VP(CholHS) samples in bulk and in the submicrometer particles are shown schematically in Figure 3.8. As expected from the volume fractions of PS and P4VP(CholHS), a lamellar morphology on the block copolymer level is found in bulk with all CholHS to P4VP repeat unit ratios (x) used. However, an interesting change in the packing of the side-chain P4VP(CholHS) blocks is observed as x is increased from 0.25 to 0.75. The packing changes gradually from the single CholHS layer sandwiched between P4VP rich domains at x = 0.25 to the smectic layers perpendicular to the copolymer block interfaces at x = 0.75. At low amount of CholHS side-chains, the P4VP(CholHS) blocks remain relatively flexible and allow the CholHS side-chains to microphase separate into their own phase inside the P4VP-(CholHS) domains resulting in the observed triple lamellar structure. When the amount of CholHS side chains is increased, the smectic stacking of P4VP(CholHS) block starts to dominate and the orthogonal lamellar-within-lamellar structure results.

In the submicrometer particles produced with the aerosol method at 160 °C, the lamellar bulk morphologies turn out as onion-like structures except for the P2-75CholHS particles. In the P2-75CholHS particles the copolymer domains orient perpendicularly to the particle surface. This surprising breakdown of the onion-like structure can be attributed to the increased splay deformation energy of the smectic P4VP(CholHS) domains and resulting ”stiffness” of the copolymer lamellae.

When the particles are produced at 200 °C, the amount CholHS side-chains in the P4VP domains decreases by partial mixing with the PS domains or by evaporation into the aerosol reactor. This leads to change from the onion-like to the cylindrical morphology in the P2-25CholHS particles due to decrease in the volume fraction of P4VP(CholHS). Also, the P2-75CholHS particles have the onion-like structure when produced at this temperature but it remains undecided whether this is due to isotropization of the P4VP(CholHS) domains or due to the decreased amount of CholHS in the P4VP domains.

Additionally, CholHS was successfully removed from the particles by ethanol. No significant porosity in the particles was achieved, though,

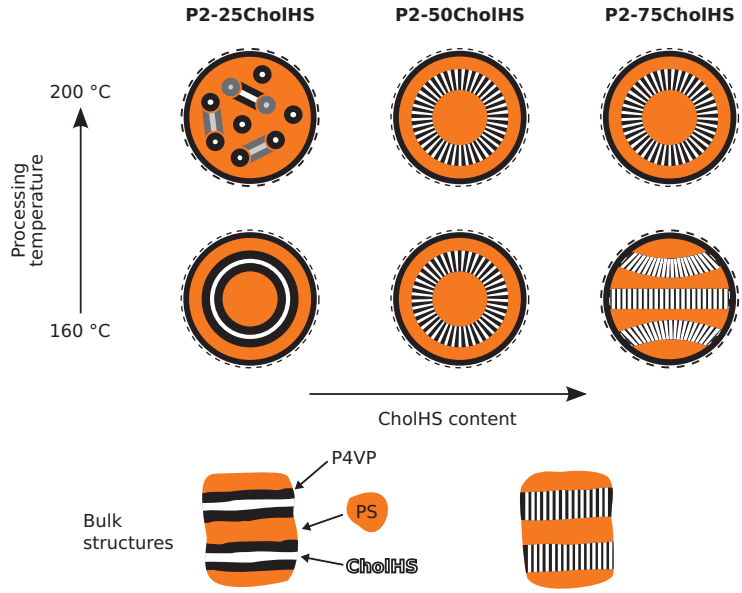

Figure 3.8. Schematic summary of the different morphologies found in the PS-P4VP(CholHS) samples in particles and in bulk. Adopted with permission from Publications III and IV. Copyright 2012 American Chemical Society.

since the remaining PS-P4VP skeleton was too soft to support the structures resulting in crumpling of the particles.

4. Induced chirality in supramolecular structures

The shapes of building blocks and their mutual interactions define the structure of a solid-state system. Sometimes, a single structural property of a building block directs the whole assembly process. This chapter and Publication V contemplates this topic, namely how chirality of constituents induces chirality into the self-organized structures of dendritic supramolecules.

4.1 Dendritic molecules

Dendritic molecules have well defined branching structures. This distinguishes them from hyperbranched polymers which have random branching and are polydisperse. The generation of a dendritic molecule tells how many levels of branches it has. With each generation, dendritic molecules became bulkier and the number of termini groups at the outer rim grows exponentially. The most basic of dendritic molecules are *dendrons* which have a tree-like wedge-shaped structure. Two or more dendrons connected from their focal points gives a *dendrimer*. Building dendrimers from different types of dendrons results in Janus-like molecules with intriguing properties.[75] Dendrons can also be polymerized into *dendronized polymers* which combine features from both dendritic molecules and linear polymers.[76, 77, 78, 79]

The well-defined structure of dendritic molecules allows them to organize in the molecular level, in some cases creating objects which can be called ”supramolecules” in a broader meaning of the term.[80, 81, 82, 83, 84, 85] These supramolecular structures of can further self-organize into periodic lattices in the mesoscale.

Additional molecules can be attached as side-groups to the termini groups of dendritic molecules using the non-covalent methods discussed in

Chapter 3. The resulting dendritic supramolecules yield unconventional mesoscale structures in which the morphology and periodicity can be fine tuned by the dendritic generation or by the size of the side-groups. [86, 87, 88, 89, 90, 91] Some of these materials have anomalous ”inverted” structures where the side-chains are confined in domains whose curvature conflicts with the natural shape of the supramolecules. [88, 89, 90, 91]

4.2 Induced chirality in dendritic supramolecules

Chiral molecules are not superposable on their mirror images. The different mirror images are often called enantiomers and pairs of chiral molecules referred to as ”left” and ”right handed”. Chirality plays a central role in many applications. In biological systems, for example, certain types of molecules are almost always of the same handedness.

Chiral components may induce chirality to conformations of molecules or molecular assemblies. [92] Even small excess of one handedness may drive the whole system to a single chiral state in a phenomenon known as chirality amplification. [93, 94] Yashima et al. pioneered the study of memorization of the chiral state. [95] They showed that in solutions, a chiral conformation of a host polymeric molecule induced by chiral guests was retained after the guests were changed to achiral ones. Since then the effect has been shown to work with a variety of hosts such as small molecules [96], several polymers [97, 98, 99, 100, 101, 102, 103, 104, 105] and other supramolecular assemblies [106].

Chirality can be introduced into supramolecular assemblies of dendritic molecules by including chiral elements to the dendritic building blocks. Percec et al. have studied the relationship between molecular architecture and the resulting structures by synthesizing extensive series of dendritic molecules. [107, 108, 109, 110, 79, 111, 112] Among other things, they found that the molecules self-organized into chiral columns or spheres or into lamellar morphologies depending on their effective shape.

In this part of the thesis, we study how guest molecules induce chirality to dendritic hosts in the solid state. Homochiral cholesteryl sulfate molecules (CholSO, Figure 4.1) are ionically bonded to the termini groups of three generations of different dendritic molecules shown in Figures 4.1 and 4.2: dendrons D1 – D3, dendronized polymers DP1 – DP3 and dendrimers M1 – M3. The dendritic molecules share exactly the same branching unit with each other creating a homologous series of nine cases of

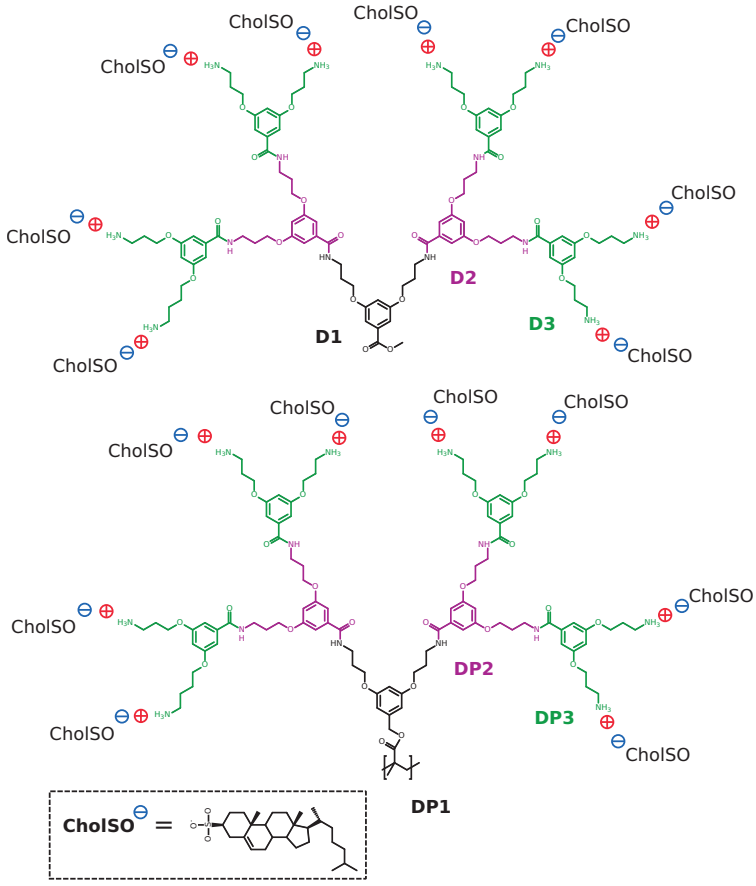

Figure 4.1. Chemical structures of dendrons D1, D2 and D3, dendronized polymers DP1, DP2 and DP3 and cholesteryl sulfate CholSO and their ionic bonding. Only the third generation molecules are entirely drawn. The corresponding first and second generations (excluding ammonium charges) are highlighted in black for first and in purple for second generation.

cholesteryl sulfate-dendritic host supramolecules. The CholSO molecules bind non-covalently to the amine-terminated termini groups of the dendritic molecules by exchanging the proton of the sulfuric acid group. Compared to Chapter 3 where the amount of the CholHS side-chains in the PS-P4VP(CholHS) diblock copolymers was varied, here the CholSO to termini group ratio of 1.00 is always used.

Some features common to all of the dendritic supramolecules studied here are present in the supramolecular dendrons as well. Figure 4.3 shows SAXS intensity data and TEM images of the dendritic supramolecules D1-CholSO, D2-CholSO and D3-CholSO. The morphology of the first generation D1-CholSO is lamellar as evident from the equally spaced SAXS peaks in Figure 4.3a and the TEM image in Figure 4.3b. The

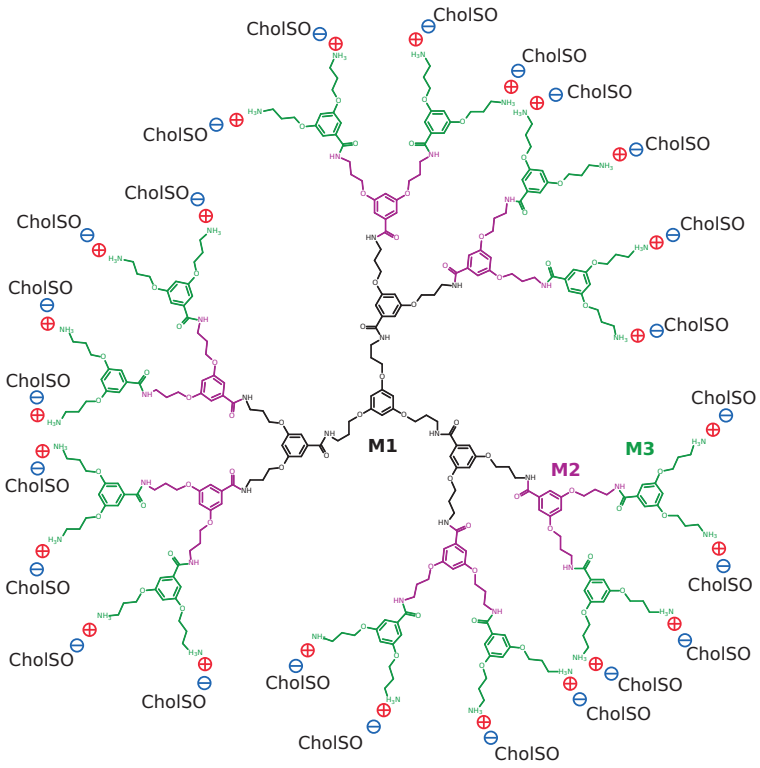

Figure 4.2. Chemical structures of dendrimers M1, M2 and M3. Only the third generation molecules are entirely drawn. The corresponding first and second generations (excluding ammonium charges) are highlighted in black for first and in purple for second generation.

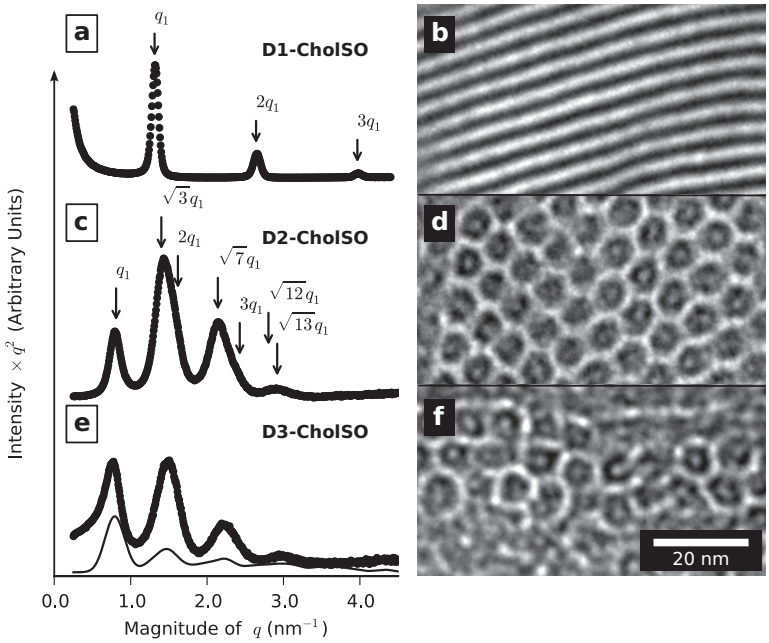

Figure 4.3. a) SAXS intensity curve and b) TEM image of the solid state structure of supramolecular dendrons D1-CholSO, c) SAXS curve and d) TEM image of D2-CholSO and e) SAXS curve and f) TEM image of D3-CholSO. The thin solid line in e) is a simulated scattering intensity. Ruthenium tetroxide staining renders the branching units dark in the TEM images. Adopted with permission from Publication V. Copyright 2010 American Chemical Society.

position of the first-order scattering peak (q_1) is 1.31 nm^{-1} giving a lamellar spacing of 4.8 nm. In the second generation dendron supramolecule D2-CholSO, the morphology changes to columnar as the TEM image in Figure 4.3d shows. SAXS data, shown in Figure 4.3c, has scattering peaks at $1 : \sqrt{3} : 2 : \sqrt{7} : 3 : \sqrt{13}$ times the first order peak at q_1. This is characteristic for hexagonal packing of the columns. The position of the first order peak gives a lattice parameter of 8.8 nm for the structure. The structure of the the third generation D3-CholSO seen in the TEM image in Figure 4.3f resembles the columnar structure of D2-CholSO. However, compared to the second generation dendron, D3-CholSO is less ordered. This can also be observed in the SAXS data in Figure 4.3e where the positions of the scattering peaks do not match with the common hexagonal pattern. To find the correct packing of the columns, parameters of an oblique columnar packing model were fitted to the measured SAXS data resulting in the simulated scattering curve shown in Figure 4.3e. The fit gives an almost hexagonal lattice for the columns with lattice parameters a = 9.9 nm, b = 8.8 nm and γ = 124°.

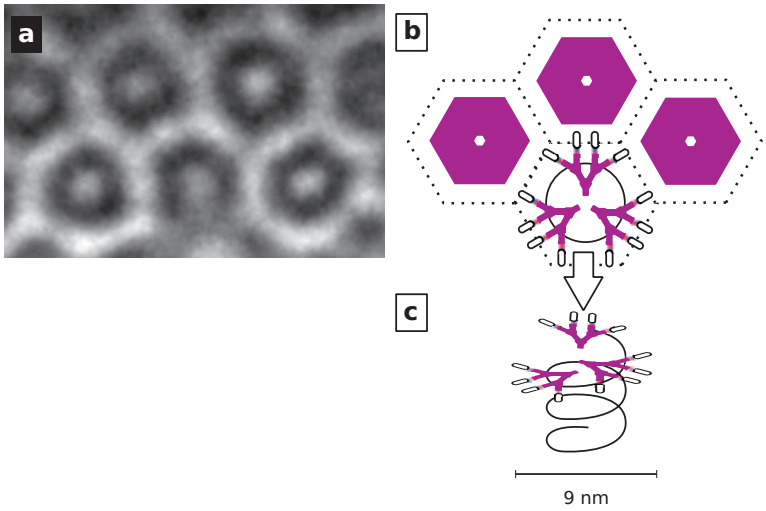

Figure 4.4. Proposed packing of dendritic supramolecules into the columnar honeycomb-like structure. a) TEM image of the columns in D2-CholSO. b) The columns consist of CholSO walls which form a honeycomb-like pattern and dendritic core in which the focal points of the dendritic molecules are in the center of the column. c) Along the column axis, the dendritic supramolecules stack around a chiral helix. Parts of the figure reprinted with permission from Publication V. Copyright 2010 American Chemical Society.

A careful look at the TEM images of the supramolecular dendrons D2-CholSO and D3-CholSO shown in Figures 4.3d and f shows a bright electron intensity spot in the center of the each column. As the ruthenium tetroxide staining turns the dendron parts of the supramolecules dark in the TEM images, we expect the bright parts of the TEM images to correspond to the CholSO molecules or voids. However, the latter case can be ruled out as gas adsorption measurements did not show any signs of porosity in the samples. Molecular packing and volume fraction consideration do not support the idea of the spots consisting of CholSO molecules. Even the size of the spots appears too small to accommodate them. Thus it seems that the CholSO molecules occupy the continuous honeycomb-like walls of the columns while the centers of the columns consist of the focal points of the dendrons. When the chirality of the columns discussed later is taken into account, the molecular packing schematically shown in Figure 4.4 can be proposed. In the proposed packing, the focal points of the dendron supramolecules point to the center of the columns while the CholSO molecules point outward. The molecules stack around a helical path on top of each other. This stacking is the source of the supramolecular chirality.

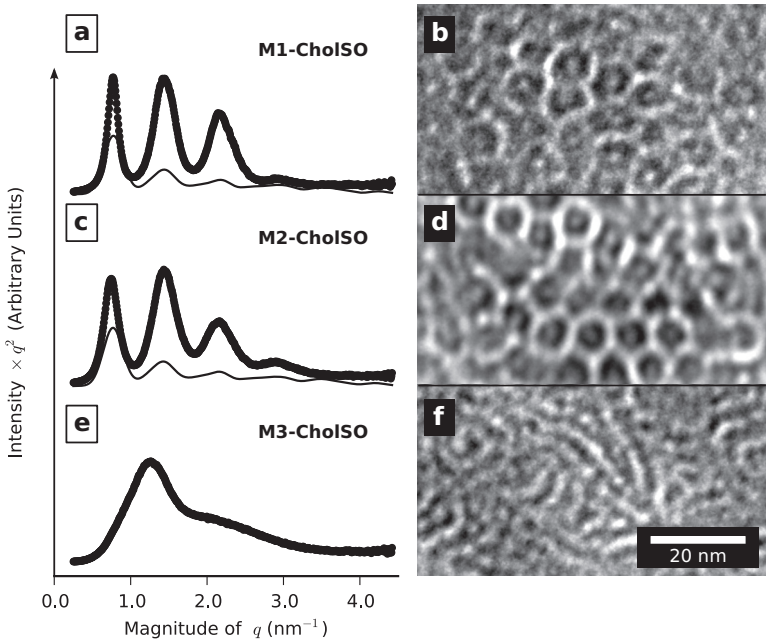

Figure 4.5. a) SAXS intensity curve and b) TEM image of the solid-state structure of the supramolecular dendrimers M1-CholSO, c) SAXS curve and d) TEM image of M2-CholSO and e) SAXS curve and f) TEM image of M3-CholSO. The thin solid lines in a) and c) are simulated scattering intensities. Ruthenium tetroxide staining renders the branching units dark in the TEM images. Adopted with permission from Publication V. Copyright 2010 American Chemical Society.

The a and b lattice parameters of the supramolecular dendron D3-CholSO are surprisingly close to D2-CholSO despite the larger size of the D3-CholSO molecules. Also parameters of similar magnitude are encountered in the columnar structures of M1-CholSO and M2-CholSO as will be shown later. These similarities in the lattice parameters can be explained by the increased tilt of the dendron molecules or branches of dendrimers along the helical columns.

The columnar packing can be found from some of the supramolecular dendrimers, as well. The host dendrimers M1, M2 and M3 consist of three dendrons of the corresponding generation bonded together from their focal points by a linker group. Their shape makes dendrimers more bulky and they have less degrees of freedom than their dendron building blocks. This has direct consequences in the ordering of the self-organization process of their supramolecular counterparts M1-CholSO – M3-CholSO as shown by the SAXS data and TEM images in Figure 4.5. The structure of M1-CholSO and M2-CholSO resembles the columnar structure of D2-CholSO

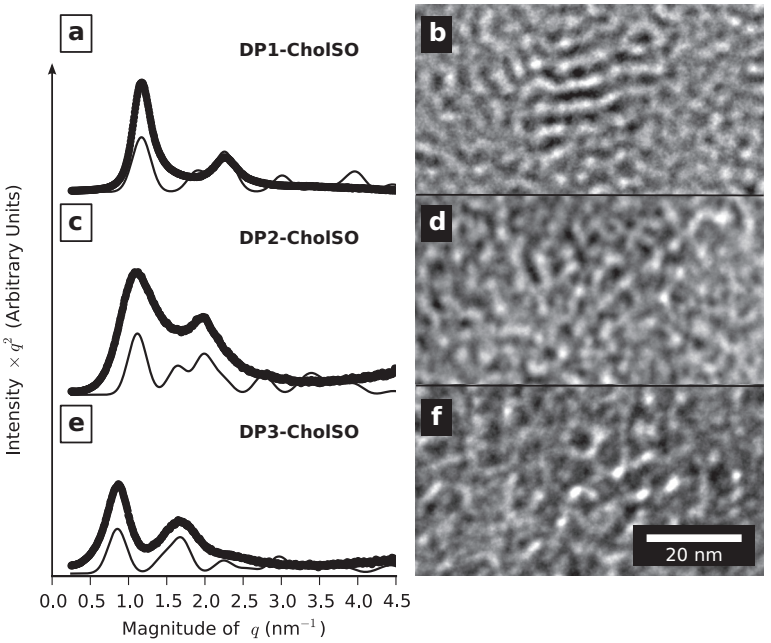

Figure 4.6. a) SAXS intensity curve and b) TEM image of the solid-state structure of the supramolecular dendronized polymers DP1-CholSO, c) SAXS curve and d) TEM image of DP2-CholSO and e) SAXS curve and f) TEM image of DP3-CholSO. The thin solid lines in the SAXS graphs are simulated scattering intensities. Ruthenium tetroxide staining renders the branching units dark in the TEM images. Adopted with permission from Publication V. Copyright 2010 American Chemical Society.

and D3-CholSO. As in the case of D3-CholSO, the packing of the columns in M1-CholSO and M2-CholSO is not purely hexagonal. Fitting to the oblique columnar model gives lattice parameters of a = 10.2 nm, b = 9.0 nm and γ = 124° for both M1-CholSO and M2-CholSO. The self-organization of the largest dendrimer, M3-CholSO is even more crippled. There is a single clear peak in the SAXS intensity curve in Figure 4.5e which indicates that a structure exists in the material. The position of the peak at 1.27 nm^{-1} corresponds to a period of 4.9 nm. However, the single diffuse shoulder peak at 2.0 – 3.0 nm^{-1} makes it difficult to assess a lattice. Also, the TEM image shown in Figure 4.5f shows only a rather disordered structure. Thus, even though the M3-CholSO molecules self-organize into periodic structures, the ordering is so poor that a definitive structure cannot be determined.

The most restricted in degrees of freedom of the dendritic molecules covered here are the dendronized polymers DP1, DP2 and DP3. Consequently, it is no surprise that the self-organization of their supramolecular

counterparts DP1-CholSO – DP3-CholSO is even more constrained than of the dendrons or dendrimers. Figure 4.6 shows the SAXS data and TEM images of DP1-CholSO – DP3-CholSO. The two scattering peaks which appear in all three samples make it evident that the supramolecules self-organize into periodic structures. In the TEM images a structure is seen as well. However, the irregular positions of the SAXS peaks or the disordered structures seen under TEM do not give out the exact structure readily. To remedy the situation, simulated scattering intensity peaks of tetragonal structures were fitted to the SAXS intensity data from all of the supramolecular dendronized polymers. The fitted data is shown in Figures 4.6a, c and e and the lattice parameters extracted from the fits are a = 5.4 nm and b = 3.3 nm for DP1-CholSO, a = 5.6 nm and b = 3.8 nm for DP2-CholSO and a = 7.4 nm and b = 4.3 nm for DP3-CholSO.

Chirality and optical properties of the supramolecules are investigated in the solid state by circular dichroism (CD) and by spectroscopy covering the ultraviolet and visible light wavelengths (UV-Vis). All the different types of dendritic molecules have similar, generation-dependent behavior. Thus, only the measurements taken from the dendrons D1 – D3, from their supramolecular counterparts D1-CholSO – D3-CholSO as well as from pure CholSO are shown in Figure 4.7. As can be seen from the Figures 4.7a, c and e, the pure dendrons D1 – D3 do not show chirality in the investigated wavelength range even though two of them absorb in the ultraviolet wavelengths (Figures 4.7b, d and f). On the other hand, pure CholSO shows a chiral response as expected (Figure 4.7a). Also, all the dendron supramolecules D1-CholSO – D3-CholSO show nonzero circular dichroism signals. However, these signal differ from that of the pure CholSO. Therefore, the molecular structures responsible for the circular dichroism must be different from that of pure CholSO suggesting the presence of supramolecular induced chirality. The CD signal is stronger for the lower generation supramolecules as well as for the lower molecular weight dendritic molecules. This indicates that molecular mobility during the self-organization process leads to more ordered structures which is important to macromolecular chirality. According to the CD analysis, the helical arrangement of the dendritic molecules shown in Figure 4.4c seems to be a reasonable interpretation of the columnar structures found in D2-CholSO, D3-CholSO, M1-CholSO, and M2-CholSO.

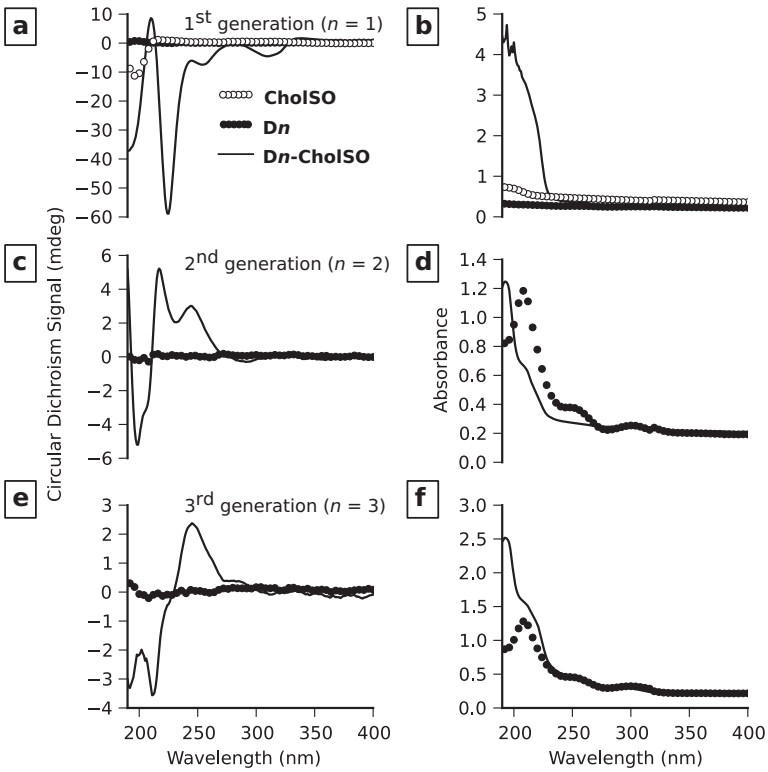

Figure 4.7. a) CD signals and b) UV-Vis spectra of pure CholSO, dendrons D1 and D1-CholSO and c) CD signals and d) UV-Vis spectra of D2 and D2-CholSO and e) CD signals and f) UV-Vis spectra of D3 and D3-CholSO. All measurements were taken from solid-state samples. Adopted with permission from Publication V. Copyright 2010 American Chemical Society.

Table 4.1. The self-organized structures of the supramolecular dendrons D1-CholSO – D3-CholSO, dendrimers M1-CholSO – M3-CholSO and dendronized polymers DP1-CholSO – DP3-CholSO.

	generation		
molecule type	1st	2nd	3rd
dendrons	lamellar	hexagonal	oblique
dendrimers	oblique	oblique	not assessed
dendronized polymers	tetragonal	tetragonal	tetragonal

4.3 Summary

The different structures the dendritic supramolecules self-organize into are summarized in Table 4.1 while their lattice parameters are collected into Table 4.2. Structure-wise the supramolecules can be divided into three groups:

1. Lamellar (D1-CholSO). The supramolecular D1-CholSO dendrons pack into alternating lamellae of dendritic cores and CholSO molecules. The CD signal, which is the most intense of all of the dendritic supramolecules studied here, may be due to undulations in the lamellae caused by the induced chirality effect.

2. Hexagonal or oblique columnar (D2-CholSO, D3-CholSO, M1-CholSO and M2-CholSO). These dendritic supramolecules self-organize into columns with the focal points in the center and the peripheral CholSO molecules in the rim, as schematically shown in Figure 4.4. The columns, in turn, are arranged into hexagonal (D2-CholSO) or close to hexagonal lattices. The bulky nature of D3-CholSO, M1-CholSO and M2-CholSO seems to cramp the packing of the columns thus leading to the ”frustrated” oblique structures. Also, the lattice parameters do not change much with the generation or the type of dendritic supramolecule which may be caused by tilting of the molecules in the columns.

3. Tetragonal columnar (DP1-CholSO, DP2-CholSO, DP3-CholSO). The restricted degrees of freedom of the polymers leads to rather poorly ordered packing of the self-organized columns. Further, the actual columns are different from the ones found in the supramolecular dendrons and dendrimers discussed above. Unfortunately, the precise self-organization of the columns cannot be clarified from the data available.

Table 4.2. Solid-state structures and lattice parameters of the supramolecular dendrons D1-CholSO – D3-CholSO, dendrimers M1-CholSO – M3-CholSO and dendronized polymers DP1-CholSO – DP3-CholSO. Adopted with permission from Publication V. Copyright 2010 American Chemical Society

supramolecule	structure	lattice parameters
dendrons		
D1-CholSO	lamellar	4.8 nm
D2-CholSO	hexagonal	$a = b = 9.0$ nm, $\gamma = 120°$
D3-CholSO	oblique	$a = 9.9$ nm, $b = 8.8$ nm, $\gamma = 124°$
dendrimers		
M1-CholSO	oblique	$a = 10.2$ nm, $b = 9.0$ nm, $\gamma = 124°$
M2-CholSO	oblique	$a = 10.2$ nm, $b = 9.0$ nm, $\gamma = 124°$
M3-CholSO	not assessed	4.7 nm
dendronized polymers		
DP1-CholSO	tetragonal	$a = 5.4$ nm, $b = 3.3$ nm
DP2-CholSO	tetragonal	$a = 5.6$ nm, $b = 3.8$ nm
DP3-CholSO	tetragonal	$a = 7.4$ nm, $b = 4.3$ nm

It has been shown here that chirality of constituents can be induced into the solid-state structures the dendritic supramolecules self-organize into. The strength of the chiral effect to optical signals depends on the ordering of the structures which in turn depends on the size and available degrees of freedom of the supramolecules. The level of ordering decreases with increasing dendritic generation and in the sequence of dendrons $\rightarrow$ dendrimers $\rightarrow$ dendronized polymers.

5. Conclusions

The subjects of self-organized templates, hierarchical structure-within-structure morphologies and induced chirality in solid state supramolecular systems were discussed in this thesis. These are examples of utilizing and controlling the self-organization processes to achieve complex structures on the molecular level and in larger length scales.

The self-organized templating method discussed in Chapter 2 exemplifies the ways to control these processes. The final morphology of the block copolymer template, that is, whether flakes or porous material will be produced, is decided by the amount of Resin added. The thickness of the flakes or the size of the mesopores, on the other hand, is decided by the total length of the templating PS-P4VP chains. An additional processing parameter is the pyrolyzation time at 420 °C which controls the ratio between micro- and mesopores. There are also functional groups at the surfaces of the final carbonaceous materials which allow further functionalization. [36, 37] These properties enable precise tailoring of the templated materials for the application at hand.

In the future, it would be interesting to expand the hierarchy of pore sizes to include macropores to further enhance mass transportation. This could be achieved, for example, by infiltrating PS colloidal crystals with the templating copolymer and Resin. Removal of the colloids during the pyrolyzation may then lead to macropores in the size range of 100 – 1000 nm.

Also, the hexagonal cylindrical morphology may not be the most optimal for mass transportation due to low interconnectivity of the resulting mesopores. This could be improved using bicontinuous morphologies, for instance. [113] However, these morphologies appear usually at narrow parameter spaces in the phase diagrams of microphase separated systems and thus may be difficult to realize.

As a gas barrier additive, the flakes studied in this thesis may have already been superseded by another emerging material, namely graphene. Graphene seems to be the perfect candidate for this application: it is atomically thin, can be produced in large sheets and it has superior barrier properties. [114] The functionalization of graphene makes compatibilization with the separation membrane matrix feasible.

However, using another exotic morphology, perforated layers, as a template to the flakes may allow them to be used as selective gas separation additives instead of plain barrier additives. Finding the correct Resin/PS-P4VP ratio to achieve the perforated morphology may prove to be difficult, though.

The complexity of the microphase separated structures can be increased by attaching side-chains to the copolymer blocks as discussed in Chapter 3. In the case of CholHS attached to PS-P4VP backbone, the P4VP(CholHS) domains pack in two distinct ways depending on the amount of CholHS. With low amount of CholHS, a novel single layer structure sandwiched between P4VP rich domains is found. Addition of CholHS side-chains gradually transforms the structure to the more conventional smectic layers perpendicular to the block domain interfaces. These morphologies are basically repeated in submicrometer particles with a strong surface effect. The spherical shape of the particles bends the block copolymer lamellae into concentric shells resulting in an onion-like domain structure. However, the onion-like morphology breaks down with high enough amount of CholHS side-chains as the bending of the block copolymer lamellae becomes energetically too expensive due to increased splay deformation energy of the smectically packed P4VP(CholHS) domains. In this case, the P4VP(CholHS) domains orient perpendicularly to the particle surface.

The triple lamellar structure with the single CholHS layer inside P4VP-(CholHS) lamellae reported for the first time in Publication III is an intriguing morphology. It may be used, for example, to precisely position nanoparticles within the block copolymer morphology.

The block copolymer morphology perpendicular to a surface found in the high CholHS content particles may affect how molecules diffuse in and out of the particles compared to the onion-like morphology. This effect is key to applications such as drug release and needs to be addressed in further studies.

One may also ask how the PS-P4VP templated Resin behaves in par-

ticles discussed above. Because the cured Resin and the carbonaceous material resulting from the pyrolyzation process are hard, they may not crumple as the PS-P4VP(CholHS) particles after selective removal of CholHS as reported in Chapter 3. In fact, this idea has been already put to test. Preliminary results show that curing of the particles needs to be thought out carefully as the residence time in the reactor is too short for curing and heating the particles after collection leads to melting.

A different aspect of the influence of non-covalently attached molecules to the formation of solid-state structures was explored in Chapter 4: induced chirality. The study underlines the importance of unhindered mobility and available degrees of freedom of the building blocks to achieve well-organized supramolecular assemblies.

Bibliography

[1] H. Kakisawa and T. Sumitomo, *Science and Technology of Advanced Materials* **12**, 064710 (2011).

[2] L. Eisoldt, A. Smith, and T. Scheibel, *Materials Today* **14**, 80 (2011).

[3] B. Bhushan, *Langmuir* **28**, 1698 (2012).

[4] H. Fudouzi, *Science and Technology of Advanced Materials* **12**, 064704 (2011).

[5] R. Ulrich, A. D. Chesne, M. Templin, and U. Wiesner, *Advanced Materials* **11**, 141 (1999).

[6] P. F. W. Simon, R. Ulrich, H. W. Spiess, and U. Wiesner, *Chemistry of Materials* **13**, 3464 (2001).

[7] S. Renker, S. Mahajan, D. T. Babski, I. Schnell, A. Jain, J. Gutmann, Y. Zhang, S. M. Gruner, H. W. Spiess, and U. Wiesner, *Macromolecular Chemistry and Physics* **205**, 1021 (2004).

[8] D. M. Dabbs and I. A. Aksay, *Annual Review of Physical Chemistry* **51**, 601 (2000).

[9] Y. Meng, D. Gu, F. Zhang, Y. Shi, H. Yang, Z. Li, C. Yu, B. Tu, and D. Zhao, *Angewandte Chemie International Edition* **44**, 7053 (2005).

[10] Y. Wan, Y. Shi, and D. Zhao, *Chemistry of Materials* **20**, 932 (2008).

[11] A. H. Lu and F. Schüth, *Advanced Materials* **18**, 1793 (2006).

[12] H. M. C. de Azeredo, *Food Research International* **42**, 1240 (2009).

[13] C. Silvestre, D. Duraccio, and S. Cimmino, *Progress in Polymer Science* **36**, 1766 (2011).

[14] T. V. Duncan, *Journal of Colloid and Interface Science* **363**, 1 (2011).

[15] R. K. Bharadwaj, *Macromolecules* **34**, 9189 (2001).

[16] C. Lu and Y. Mai, *Physical Review Letters* **95**, 088303 (2005).

[17] K. Bhunia, S. Dhawan, and S. S. Sablani, *Journal of Food Science* **77**, N29 (2012).

[18] D. R. Paul and L. M. Robeson, *Polymer* **49**, 3187 (2008).

[19] J. Gaume, C. Taviot-Gueho, S. Cros, A. Rivaton, S. Therias, and J.-L. Gardette, *Solar Energy Materials and Solar Cells* **99**, 240 (2012).

[20] C. Felice, S. Ye, and D. Qu, *Industrial & Engineering Chemistry Research* **49**, 1514 (2010).

[21] L. Unnikrishnan, S. Mohanty, S. K. Nayak, and N. Singh, *Journal of Applied Polymer Science* **124**, E309 (2012).

[22] M. Bhattacharya, S. Biswas, S. Bandyopadhyay, and A. K. Bhowmick, *Polymers for Advanced Technologies* **23**, 596 (2012).

[23] C. Liang, Z. Li, and S. Dai, *Angewandte Chemie International Edition* **47**, 3696 (2008).

[24] D. Q. Vu, W. J. Koros, and S. J. Miller, *Journal of Membrane Science* **211**, 311 (2003).

[25] M. Das, J. D. Perry, and W. J. Koros, *Industrial & Engineering Chemistry Research* **49**, 9310 (2010).

[26] D. Saha and S. Deng, *Langmuir* **25**, 12550 (2009).

[27] G. P. Hao, W. C. Li, D. Qian, G. H. Wang, W. Zhang, T. Zhang, A. Wang, F. Schueth, H. J. Bongard, and A. H. Lu, *Journal of the American Chemical Society* **133**, 11378 (2011).

[28] Y. S. Hu, P. Adelhelm, B. M. Smarsly, S. Hore, M. Antonietti, and J. Maier, *Advanced Functional Materials* **17**, 1873 (2007).

[29] M. C. Gutiérrez, F. Picó, F. Rubio, J. M. Amarilla, F. J. Palomares, M. L. Ferrer, F. del Monte, and J. M. Rojo, *Journal of Materials Chemistry* **19**, 1236 (2009).

[30] K. Wang, Y. Wang, Y. Wang, E. Hosono, and H. Zhou, *The Journal of Physical Chemistry C* **113**, 1093 (2009).

[31] P. Bernardo, E. Drioli, and G. Golemme, *Industrial & Engineering Chemistry Research* **48**, 4638 (2009).

[32] P. S. Goh, A. F. Ismail, S. M. Sanip, B. C. Ng, and M. Aziz, *Separation and Purification Technology* **81**, 243 (2011).

[33] H.-K. Jeong, W. Krych, H. Ramanan, S. Nair, E. Marand, and M. Tsapatsis, *Chemistry of Materials* **16**, 3838 (2004).

[34] O. K. Farha, I. Eryazici, N. C. Jeong, B. G. Hauser, C. E. Wilmer, A. A. Sarjeant, R. Q. Snurr, S. T. Nguyen, A. O. Yazaydin, and J. T. Hupp, *Journal of the American Chemical Society* **134**, 15016 (2012).

[35] M. Hartmann, *Angewandte Chemie International Edition* **43**, 5880 (2004).

[36] H. Kosonen, S. Valkama, A. Nykänen, M. Toivanen, G. ten Brinke, J. Ruokolainen, and O. Ikkala, *Advanced Materials* **18**, 201 (2006).

[37] S. Valkama, A. Nykänen, H. Kosonen, R. Ramani, F. Tuomisto, P. Engelhardt, G. ten Brinke, O. Ikkala, and J. Ruokolainen, *Advanced Functional Materials* **17**, 183 (2007).

[38] J. Ruokolainen, M. Torkkeli, R. Serimaa, E. Komanschek, G. ten Brinke, and O. Ikkala, *Macromolecules* **30**, 2002 (1997).

[39] J. D. Fox and S. J. Rowan, *Macromolecules* **42**, 6823 (2009).

[40] L. S. Shimizu, *Polymer International* **56**, 444 (2007).

[41] J. M. Pollino and M. Weck, *Chemical Society Reviews* **34**, 193 (2005).

[42] M. Weck, *Polymer International* **56**, 453 (2007).

[43] M. R. Hammond and R. Mezzenga, *Soft Matter* **4**, 952 (2008).

[44] S. Malik, P. K. Dhal, and R. A. Mashelkar, *Macromolecules* **28**, 2159 (1995).

[45] J. Ruokolainen, G. ten Brinke, O. Ikkala, M. Torkkeli, and R. Serimaa, *Macromolecules* **29**, 3409 (1996).

[46] J. T. Korhonen, T. Verho, P. Rannou, and O. Ikkala, *Macromolecules* **43**, 1507 (2010).

[47] H. R. Thomas and J. J. O'Malley, *Macromolecules* **12**, 323 (1979).

[48] H. Hasegawa and T. Hashimoto, *Macromolecules* **18**, 589 (1985).

[49] G. H. Fredrickson, *Macromolecules* **20**, 2535 (1987).

[50] C. R. Stewart-Sloan and E. L. Thomas, *European Polymer Journal* **47**, 630 (2011).

[51] H. Fischer and S. Poser, *Acta Polymerica* **47**, 413 (1996).

[52] E. L. Thomas, J. T. Chen, M. J. E. O'Rourke, C. K. Ober, and G. Mao, *Macromolecular Symposium* **117**, 241 (1997).

[53] S. Poser, H. Fischer, and M. Arnold, *Progress in Polymer Science* **23**, 1337 (1998).

[54] J. Ruokolainen, G. ten Brinke, and O. Ikkala, *Advanced Materials* **11**, 777 (1999).

[55] J. Ruokolainen, M. Saariaho, O. Ikkala, G. ten Brinke, E. L. Thomas, M. Torkkeli, and R. Serimaa, *Macromolecules* **32**, 1152 (1999).

[56] A. F. Thünemann and S. General, *Macromolecules* **34**, 6978 (2001).

[57] O. Ikkala and G. ten Brinke, *Chemical Communications* **(19)**, 2131 (2004).

[58] S. Bondzic, J. de Wit, E. Polushkin, A. J. Schouten, G. ten Brinke, J. Ruokolainen, O. Ikkala, I. Dolbnya, and W. Bras, *Macromolecules* **37**, 9517 (2004).

[59] B. Nandan, C. H. Lee, H. L. Chen, and W. C. Chen, *Macromolecules* **38**, 10117 (2005).

[60] W.-S. Chiang, C.-H. Lin, B. Nandan, C.-L. Yeh, M. H. Rahman, W.-C. Chen, and H.-L. Chen, *Macromolecules* **41**, 8138 (2008).

[61] C. S. Tsao and H. L. Chen, *Macromolecules* **37**, 8984 (2004).

[62] S. Valkama, T. Ruotsalainen, A. Nykänen, A. Laiho, H. Kosonen, G. ten Brinke, O. Ikkala, and J. Ruokolainen, *Macromolecules* **39**, 9327 (2006).

[63] S. Bondzic, E. Polushkin, J. Ruokolainen, and G. ten Brinke, *Polymer* **49**, 2669 (2008).

[64] S. Naidu, H. Ahn, H. Lee, Y. M. Jung, and D. Y. Ryu, *Macromolecules* **43**, 6120 (2010).

[65] R. Mäki-Ontto, K. de Moel, W. de Odorico, J. Ruokolainen, M. Stamm, G. ten Brinke, and O. Ikkala, *Advanced Materials* **13**, 117 (2001).

[66] D. Zschech, A. P. Milenin, R. Scholz, R. Hillebrand, Y. Sun, P. Uhlmann, M. Stamm, M. Steinhart, and U. Gösele, *Macromolecules* **40**, 7752 (2007).

[67] B. Nandan, E. B. Gowd, N. C. Bigall, A. Eychmüller, P. Formanek, P. Simon, and M. Stamm, *Advanced Functional Materials* **19**, 2805 (2009).

[68] S. Valkama, H. Kosonen, J. Ruokolainen, T. Haatainen, M. Torkkeli, R. Serimaa, G. ten Brinke, and O. Ikkala, *Nature materials* **3**, 872 (2004).

[69] C. Osuji, C.-Y. Chao, I. Bita, C. K. Ober, and E. L. Thomas, *Advanced Functional Materials* **12**, 753 (2002).

[70] R. Deng, S. Liu, J. Li, Y. Liao, J. Tao, and J. Zhu, *Advanced Materials* **14**, 1889 (2012).

[71] Y. Mogi, M. Nomura, H. Kotsuji, K. Ohnishi, Y. Matsushita, and I. Noda, *Macromolecules* **27**, 6755 (1994).

[72] R. Stadler, C. Auschra, J. Beckmann, U. Krappe, I. Voight-Martin, and L. Leibler, *Macromolecules* **28**, 3080 (1995).

[73] T. S. Bailey, H. D. Pham, and F. S. Bates, *Macromolecules* **34**, 6994 (2001).

[74] F. Schacher, J. Yuan, H. G. Schoberth, and A. H. E. Müller, *Polymer* **51**, 2021 (2010).

[75] V. Percec, D. A. Wilson, P. Leowanawat, C. J. Wilson, A. D. Hughes, M. S. Kaucher, D. A. Hammer, D. H. Levine, A. J. Kim, F. S. Bates, K. P. Davis, T. P. Lodge, M. L. Klein, R. H. DeVane, E. Aqad, B. M. Rosen, A. O. Argintaru, M. J. Sienkowska, K. Rissanen, S. Nummelin, and J. Ropponen, *Science* **328**, 1009 (2010).

[76] A. D. Schlüter and J. P. Rabe, *Angewandte Chemie International Edition* **39**, 864 (2000).

[77] A. Zhang, L. Shu, Z. Bo, and A. D. Schlüter, *Macromolecular Chemistry and Physics* **204**, 328 (2003).

[78] H. Frauenrath, *Progress in Polymer Science* **30**, 325 (2005).

[79] J. G. Rudick and V. Percec, *Accounts of Chemical Research* **41**, 1641 (2008).

[80] F. Vögtle, S. Gestermann, R. Hesse, H. Schwierz, and B. Windisch, *Progress in Polymer Science* **25**, 987 (2000).

[81] D. A. Tomalia, *Progress in Polymer Science* **30**, 294 (2005).

[82] J. Barbera, B. Donnio, L. Gehringer, D. Guillon, M. Marcos, A. Omenat, and J. L. Serrano, *Journal of Materials Chemistry* **15**, 4093 (2005).

[83] K. T. Al-Jamal, C. Ramaswamy, and A. T. Florence, *Advanced Drug Delivery Reviews* **57**, 2238 (2005).

[84] D. K. Smith, A. R. Hirst, C. S. Love, J. G. Hardy, S. V. Brignell, and B. Huang, *Progress in Polymer Science* **30**, 220 (2005).

[85] B. M. Rosen, C. J. Wilson, D. A. Wilson, M. Peterca, M. R. Imam, and V. Percec, *Chemical reviews* **109**, 6275 (2009).

[86] N. Canilho, E. Kasëmi, R. Mezzenga, and A. D. Schlüter, *Journal of the American Chemical Society* **128**, 13998 (2006).

[87] N. Canilho, E. Kasëmi, A. D. Schlüter, and R. Mezzenga, *Macromolecules* **40**, 2822 (2007).

[88] N. Canilho, E. Kasëmi, A. D. Schlüter, J. Ruokolainen, and R. Mezzenga, *Macromolecules* **40**, 7609 (2007).

[89] N. Canilho, E. Kasëmi, A. D. Schlüter, J. Ruokolainen, and R. Mezzenga, *Macromolecular Symposia* **270**, 58 (2008).

[90] W. B. Lee, R. Elliott, R. Mezzenga, and G. H. Fredrickson, *Macromolecules* **42**, 849 (2009).

[91] R. Mezzenga, J. Ruokolainen, N. Canilho, E. Kasëmi, D. A. Schlüter, W. B. Lee, and G. H. Fredrickson, *Soft Matter* **5**, 92 (2009).

[92] G. A. Hembury, V. V. Borovkov, and Y. Inoue, *Chemical reviews* **108**, 1 (2008).

[93] M. M. Green, J.-W. Park, T. Sato, A. Teramoto, S. Lifson, R. L. B. Selinger, and J. V. Selinger, *Angewandte Chemie International Edition* **38**, 3138 (1999).

[94] B. L. Feringa and R. A. van Delden, *Angewandte Chemie International Edition* **38**, 3418 (1999).

[95] E. Yashima, K. Maeda, and Y. Okamoto, *Nature* **399**, 449 (1999).

[96] R. D. Rasberry, X. Wu, B. N. Bullock, M. D. Smith, and K. D. Shimizu, *Organic letters* **11**, 2599 (2009).

[97] Z. Yu, X. Wan, H. Zhang, X. Chen, and Q. Zhou, *Chemical Communications* , 974 (2003).

[98] M. Ishikawa, K. Maeda, Y. Mitsutsuji, and E. Yashima, *Journal of the American Chemical Society* **126**, 732 (2004).

[99] K. Maeda, K. Morino, Y. Okamoto, T. Sato, and E. Yashima, *Journal of the American Chemical Society* **126**, 4329 (2004).

[100] K. Morino, T. Asari, K. Maeda, and E. Yashima, *Journal of Polymer Science Part A: Polymer Chemistry* **42**, 4711 (2004).

[101] K. Morino, N. Watase, K. Maeda, and E. Yashima, *Chemistry - A European Journal* **10**, 4703 (2004).

[102] H. Onouchi, D. Kashiwagi, K. Hayashi, K. Maeda, and E. Yashima, *Macromolecules* **37**, 5495 (2004).

[103] H. Onouchi, T. Miyagawa, A. Furuko, K. Maeda, and E. Yashima, *Journal of the American Chemical Society* **127**, 2960 (2005).

[104] T. Hasegawa, K. Maeda, H. Ishiguro, and E. Yashima, *Polymer Journal* **38**, 912 (2006).

[105] Y. Hase, M. Ishikawa, R. Muraki, K. Maeda, and E. Yashima, *Macromolecules* **39**, 6003 (2006).

[106] T. Ishi-i, M. Crego-Calama, P. Timmerman, D. N. Reinhoudt, and S. Shinkai, *Journal of the American Chemical Society* **124**, 14631 (2002).

[107] V. Percec, A. E. Dulcey, V. S. K. Balagurusamy, Y. Miura, J. Smidrkal, M. Peterca, S. Nummelin, U. Edlund, S. D. Hudson, P. A. Heiney, H. Duan, S. N. Magonov, and S. A. Vinogradov, *Nature* **430**, 764 (2004).

[108] V. Percec, A. E. Dulcey, M. Peterca, M. Ilies, S. Nummelin, M. J. Sienkowska, and P. A. Heiney, *Proceedings of the National Academy of Sciences of the United States of America* **103**, 2518 (2006).

[109] V. Percec, J. G. Rudick, M. Peterca, E. Aqad, M. R. Imam, and P. A. Heiney, *Journal of Polymer Science Part A: Polymer Chemistry* **45**, 4974 (2007).

[110] V. Percec, M. Peterca, J. G. Rudick, E. Aqad, M. R. Imam, and P. A. Heiney, *Chemistry - A European Journal* **13**, 9572 (2007).

[111] V. Percec, M. R. Imam, M. Peterca, D. A. Wilson, and P. A. Heiney, *Journal of the American Chemical Society* **131**, 1294 (2009).

[112] V. Percec, M. R. Imam, M. Peterca, D. A. Wilson, R. Graf, H. W. Spiess, V. S. K. Balagurusamy, and P. A. Heiney, *Journal of the American Chemical Society* **131**, 7662 (2009).

[113] F. Zhang, Y. Meng, D. Gu, Yan, C. Yu, B. Tu, and D. Zhao, *Journal of the American Chemical Society* **127**, 13508 (2005).

[114] B. Ozbas, C. D. O'Neill, R. A. Register, I. A. Aksay, R. K. Prud'homme, and D. H. Adamson, *Journal of Polymer Science Part B-Polymer Physics* **50**, 910 (2012).

[115] S. Zhou, H. Hu, C. Burger, and B. Chu, *Macromolecules* **34**, 1772 (2001).

Aalto-DD 24/2013

ISBN 978-952-60-5012-6
ISBN 978-952-60-5013-3 (pdf)
ISSN-L 1799-4934
ISSN 1799-4934
ISSN 1799-4942 (pdf)

Aalto University
School of Science
Department of Applied Physics
www.aalto.fi

BUSINESS +
ECONOMY

ART +
DESIGN +
ARCHITECTURE

SCIENCE +
TECHNOLOGY

CROSSOVER

**DOCTORAL
DISSERTATIONS**